Monthly Notices
of the
ROYAL ASTRONOMICAL SOCIETY

Mon. Not. R. Astron. Soc. **403,** 1296–1316 (2010) doi:10.1111/j.1365-2966.2009.16187.x

The spectral–temporal properties of the prompt pulses and rapid decay phase of gamma-ray bursts

R. Willingale,[1⋆] F. Genet,[2,3] J. Granot[2] and P. T. O'Brien[1]

[1]*Department of Physics and Astronomy, University of Leicester, Leicester LE1 7RH*
[2]*Center for Astrophysics Research, University of Hertfordshire, Hatfield AL10 9AB*
[3]*Racah Institute of Physics, Hebrew University of Jerusalem, Israel*

Accepted 2009 December 8. Received 2009 November 13; in original form 2009 September 18

ABSTRACT

The prompt emission from gamma-ray burst is the brightest electromagnetic emission known, yet its origin is not understood. The flux density of individual prompt pulses of a GRB can be represented by an analytical expression derived assuming the emission is from a thin, ultrarelativistically expanding, uniform, spherical shell over a finite range of radii. We present the results of fitting this analytical expression to the light curves from the four standard *Swift* Burst Alert Telescope energy bands and two standard *Swift* X-ray Telescope energy bands of 12 bursts. The expression includes the high latitude emission (HLE) component and the fits provide a rigorous demonstration that the HLE can explain the rapid decay phase of the prompt emission. The model also accommodates some aspects of energy-dependent lag and energy-dependent pulse width, but there are features in the data which are not well represented. Some pulses have a hard, narrow peak which is not well fitted or a rise and decay which are faster than expected using the standard indices derived assuming synchrotron emission from internal shocks, although it might be possible to accommodate these features using a different emission mechanism within the same overall framework. The luminosity of pulses is correlated with the peak energy of the pulse spectrum, $L_f \propto [E_{\rm peak}(1+z)]^{1.8}$, and anticorrelated with the time since ejection of the pulse, $L_f \propto [T_f/(1+z)]^{-2.0}$.

Key words: radiation mechanisms: non-thermal – ISM: jets and outflows – gamma-rays: bursts.

1 INTRODUCTION

The ability of the *Swift* satellite (Gehrels et al. 2004) to rapidly and autonomously slew when the Burst Alert Telescope [BAT; energy range 15–350 keV (Barthelmy et al. 2005)] detects a gamma-ray burst (GRB) enables it to point the X-Ray Telescope [XRT; energy range 0.3–10 keV (Burrows et al. 2005)] at the target within ≈100 s of the trigger. For many bursts, the combination of the BAT and XRT provides continuous broad-band coverage of the prompt emission to the onset of the afterglow. A rapid decay phase (RDP) immediately following the prompt emission is observed for the majority of bursts (Nousek et al. 2006) and this decay appears as a smooth continuation of the prompt, both temporally and spectrally (O'Brien et al. 2006). This strongly suggests that the decay is the tail of the prompt emission and several models have been proposed to account for the decay (see Zhang, Liang & Zhang 2007 and references therein), but the most popular is so-called high latitude emission (HLE) or 'naked' GRB emission (Kumar & Panaitescu 2000). If the prompt emission from an expanding quasi-spherical shell suddenly turns off then radiation from increasingly larger angles relative to the line of sight continue to reach the observer because of the added path length (time delay) introduced by the curvature of the shell. The spectrum seen at later (delayed) times is subject to a smaller Doppler shift and the flux decays rapidly as the radiation is beamed away from our line of sight, leading to a simple predicted relation between the temporal decay index and the spectral index, $\alpha = 2 + \beta$ where $F_\nu(t) \propto t^{-\alpha}\ \nu^{-\beta}$, that should hold at late times when $t - t_0 \gg \Delta t$, where t_0 and Δt are the start time and width of the pulse, respectively.

Several authors have attempted to demonstrate that the RDP is consistent with the expectations of HLE (Butler & Kocevski 2007; Zhang et al. 2007) but simplifying assumptions about t_0 and Δt have to be made to allow comparison of the model predictions and the observations. Usually, a parametrized form based on the late-time asymptotic behaviour of the HLE from a single spike or pulse in the prompt light curve is assumed although it is used near the peak of the pulse before the asymptotic form is appropriate and the zero time for the power-law decay is chosen in an arbitrary way. Furthermore, most bursts consist of several prompt pulses which somehow combine to produce the single HLE tail. About 25 per cent of decays have no significant spectral evolution and

⋆E-mail: rw@star.le.ac.uk

Zhang et al. (2007) suggest these are dominated by a simple curvature effect while the rest show a clear hard-to-soft change as the flux decays which they modelled using an evolving exponential spectrum in which the cut-off energy $E_c = E_0(t/t_0 - 1)^{-\alpha_2}$. What is required is a theoretical model that incorporates the pulse profile, the evolution of the pulse spectrum, the late HLE tail and summation of the emission from several pulses so that the smooth continuation of the flux from the prompt phase in different energy bands can be predicted and compared with the BAT and XRT energy-resolved light curves. Such a model could be used to fit both prompt pulses seen by the BAT and later soft flares seen by the XRT in a consistent way. Our primary aim was to test whether or not the HLE component incorporated into a physically realistic model could explain the RDP in a rigorous way but in addition we also confront other aspects of the model with the data. We have used the analytical expression for the temporal–spectral profile of individual prompt pulses from Genet & Granot (2009) which is largely based on Sari (1998), Granot (2005) and Granot, Cohen-Tanugi & do Couto e Silva (2008). Full details about the model including a comparison with past attempts to model the RDP with HLE and the properties of the model pulses are given in Genet & Granot (2009).

Here, we present a first attempt at fitting this model to the *Swift* BAT and XRT light curves of GRBs. We have selected 12 objects using the following criteria: early coverage from the XRT including a good measurement of the RDP; relatively simple BAT light curves; overlapping or near contiguous data from the BAT and XRT giving good coverage of the transition from the prompt emission into the RDP and an absence of large X-ray flares which may obscure the RDP.

2 THE MODEL FUNCTION

Each individual peak or pulse in the prompt light curve is assumed to originate from an expanding thin shell ejected from the central engine modelled using the emission profile given by Genet & Granot (2009). For the case where the Lorentz factor of the expansion, Γ, is constant with radius (coasting index $m = 0$ where $\Gamma^2 \propto R^{-m}$), the luminosity from within the shell in the comoving frame (indicated by the primed variables) is $L'_{\nu'} = L'_0(R/R_0)^a S(\nu'/\nu'_p).S(x)$ is assumed to be the Band function (Band et al. 1993) and the peak frequency of the νF_ν spectrum is $\nu'_p = \nu'_0(R/R_0)^d$. Under the standard internal shock model, the index d is linked with the fact that the emission process is synchrotron. Assuming the fast cooling regime the peak frequency of the νF_ν spectrum is $\nu'_m \propto B'\,\gamma_m^2$ where B' is the comoving magnetic field and γ_m is the electron energy (Lorentz factor) at the peak of the spectrum. As we are in the coasting phase, the strength of shocks is roughly constant, so γ_m is constant, and then $\nu'_p = \nu'_m \propto B'$. B' is predominantly normal to the radial direction, so that $B' \approx B/\Gamma \propto B$ for $m = 0$. We expect $B \propto R^{-1}$, hence $\nu'_p \propto R^{-1}$, and thus $d = -1$. More generally, for uniform shells with a roughly constant strength of the shocks, both the rate of particles crossing the shock and the average energy per particle are constant with radius, implying a constant rate of internal energy generation $\mathrm{d}E'_{int}/\mathrm{d}t' \propto R^0$. For fast cooling, this also applies to the total comoving luminosity $L' \sim \nu'_p L'_{\nu'_p} \propto R^0$, so when $L'_{\nu'_p}$ evolves with radius so must ν'_p and we must have $d + a = 0$. In particular, this is true in the case of synchrotron emission where $d = -1$ and $a = 1$. The emission turns on when the shell is at radius R_0 and turns off at radius $R_f = R_0 + \Delta R$. If $m = 0$ and $d = -1$, we can integrate the comoving luminosity over the equal arrival time surface giving the number of photons N per unit photon energy E, area A at observed time T as

$$\frac{\mathrm{d}N}{\mathrm{d}E\,\mathrm{d}A\,\mathrm{d}T}(E, T \geq T_{\rm ej} + T_0) = P(T - T_{\rm ej}, T_f, T_{\rm rise})B\left(\frac{E}{E_f}\frac{T - T_{\rm ej}}{T_f}\right), \quad (1)$$

where the pulse profile is

$$P(T - T_{\rm ej}, T_f, T_{\rm rise}) = \left\{\left[\min\left(\frac{T - T_{\rm ej}}{T_f}, 1\right)^{a+2} - \left(\frac{T_f - T_{\rm rise}}{T_f}\right)^{a+2}\right] \times \left[1 - \left(\frac{T_f - T_{\rm rise}}{T_f}\right)^{a+2}\right]^{-1}\right\}\left(\frac{T - T_{\rm ej}}{T_f}\right)^{-1}. \quad (2)$$

The characteristic times of the pulse T_f and $T_0 = T_f - T_{\rm rise}$ are the arrival times in the observer frame of the last photon and the first photon emitted from the shell, along the line of sight, measured with respect to the ejection time, $T_{\rm ej}$. The term in square brackets in equation (2) models the rise in the pulse controlled by the temporal index a and the time-scales $T_{\rm rise}$ and T_f. The functional form of this rise is the same as in the original formulation but we have included a normalization such that the value is 1 at $T - T_{\rm ej} = T_f$ and have introduced the rise time of the pulse $T_{\rm rise}$. Fig. 1 is a schematic of the pulse profile showing the times and time-scales.

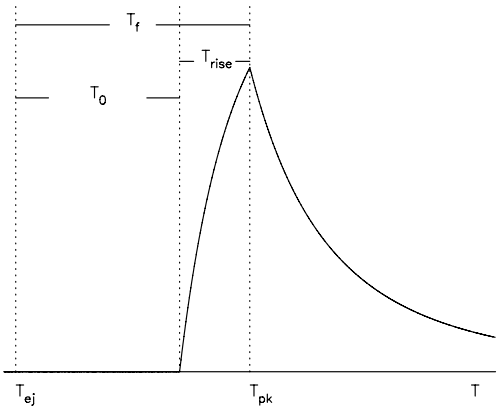

Figure 1. The pulse profile showing the times $T_{\rm ej}$ and T_{pk} and the time-scales T_f and $T_0 = T_f - T_{\rm rise}$.

$B(z)$ is the Band function with $z = (E/E_f)[(T - T_{\rm ej})/T_f\ ]^{-1}$, such that

$$B(z) = B_{\rm norm}\begin{cases} z^{b_1-1}\mathrm{e}^{-z} & z \leq b_1 - b_2 \\ z^{b_2-1}(b_1 - b_2)^{b_1-b_2}\mathrm{e}^{-(b_1-b_2)} & z > b_1 - b_2. \end{cases} \quad (3)$$

The parameters of the Band function are the normalization $B_{\rm norm}$, the low-energy spectral index b_1, the characteristic energy E_c and the high-energy spectral index b_2. The characteristic energy evolves with time, $E_c(t) = E_c(T - T_{\rm ej}) = E_f\ [(T - T_{\rm ej})/T_f\ ]^{-1}$, where E_f is the value of the cut-off energy at time $T_{pk} = T_{\rm ej} + T_f$. The peak of the $\nu F(\nu)$ spectrum at this time is $E_{\rm peak} = (b_1 + 1)E_f$. T_{pk} marks the start of the RDP and is usually the peak of the pulse as indicated in Fig. 1 although if $T_{\rm rise}$ is large, the index $d < -1$ and/or the spectrum is hard the pulse maximum can occur before T_{pk}. So, the index d in the present formulation plays a similar role to the index α_2 in Zhang et al. (2007) although we note that the formulation presented here is rigorously valid only for $d = -1$, since only in this case does the observed spectrum have the same pure Band function form as the comoving emission spectrum.

Table 1. Temporal parameters for the fitted pulses.

GRB	Pulse	T_{pk}	a	$T_{\rm rise}$	T_f	z	χ^2/d.o.f.
050724	1	0.0	1.00	1.1	(1.8, 2.1, 2.7)	0.258	1433.9/235
	2	93.4	1.00	35.0	(63.6, 66.5, 70.1)		
	3	0.50E+05	1.00	0.18E+05	(0.30E+05,0.43E+05,0.58E+05)		
050814	1	5.7	1.00	(10.5, 11.8, 14.1)	(26.4, 31.5, 37.5)	5.300	299.1/197
	2	66.4	1.00	40.0	(59.3, 64.3, 71.0)		
051001	1	−8.7	1.00	15.2	(65.1, 76.3, 91.2)		578.9/233
	2	145.7	1.00	(40.1, 42.8, 46.2)	(64.8, 69.3, 75.1)		
060211A	1	83.3	1.00	(36.2, 43.7, 47.6)	(66.9, 74.5, 80.8)		446.5/246
	2	158.6	1.00	(19.2, 21.5, 24.9)	(31.6, 35.9, 40.7)		
060814	1	10.1	1.00	13.0	(13.7, 14.3, 15.1)	0.840	2709.8/1146
	2	16.5	1.00	(3.0, 3.1, 3.3)	(9.1, 9.8, 10.4)		
	3	69.7	1.00	(8.6, 8.9, 9.1)	(25.1, 26.1, 27.2)		
	4	128.7	1.00	7.7	(34.3, 38.2, 42.8)		
	5	150.1	1.00	(67.0, 73.9, 89.0)	(232.6,252.5,279.1)		
061110A	1	8.9	1.00	(20.9, 21.9, 23.1)	(36.1, 39.2, 42.4)	0.758	417.3/ 174
	2	140.0	1.00	(71.8, 75.1, 78.9)	(154.9,165.5,176.3)		
061121	1	2.9	1.00	(2.8, 3.3, 4.2)	(4.0, 4.6, 5.7)	1.314	3052.4/630
	2	61.9	1.00	(0.9, 1.0, 1.1)	(8.6, 9.4, 10.4)		
	3	68.6	1.00	(2.1, 2.1, 2.2)	(5.9, 6.5, 7.0)		
	4	73.3	1.00	(2.2, 2.2, 2.3)	(2.8, 3.0, 3.2)		
	5	75.0	(2.10, 2.39, 2.82)	1.3	(1.5, 1.7, 2.0)		
	6	110.0	1.00	(4.5, 4.8, 5.6)	(19.5, 22.6, 27.3)		
061222A	1	1.0	1.00	5.4	(11.4, 15.1, 20.5)		2010.2/702
	2	25.7	1.00	1.0	(4.2, 5.1, 6.2)		
	3	60.0	1.00	(7.1, 7.5, 7.9)	(15.7, 17.3, 19.0)		
	4	73.8	1.00	(4.0, 4.5, 5.0)	(15.8, 17.0, 18.4)		
	5	84.7	1.00	(4.5, 5.0, 5.1)	(5.1, 5.5, 6.2)		
	6	87.1	1.00	(1.0, 1.1, 1.2)	(2.5, 2.9, 3.3)		
	7	90.0	1.00	0.5	(0.8, 1.2, 1.6)		
	8	120.0	1.00	(3.0, 5.7, 8.1)	(52.6, 65.8, 85.6)		
070420	1	−35.0	1.00	9.8	(10.6, 13.2, 16.6)		982.9/407
	2	−15.5	1.00	13.5	(14.9, 17.4, 20.0)		
	3	2.4	1.00	(7.1, 7.7, 8.3)	(13.6, 14.6, 15.6)		
	4	60.9	1.00	(12.7, 13.2, 13.9)	(18.1, 19.3, 20.5)		
070621	1	2.0	1.00	5.0	(10.4, 12.2, 14.3)		602.8/303
	2	8.0	1.00	1.2	(4.7, 7.8, 12.1)		
	3	12.0	1.00	1.9	(2.7, 4.3, 7.3)		
	4	18.0	1.00	2.8	(19.9, 21.7, 23.8)		
	5	22.0	1.00	0.8	(3.3, 5.0, 7.3)		
	6	120.8	1.00	28.3	(96.3,109.2,123.4)		
080229A	1	0.3	1.00	1.5	(7.0, 8.8, 10.8)		1494.4/ 444
	2	28.0	1.00	(1.5, 1.7, 2.0)	(5.2, 7.9, 10.6)		
	3	35.0	1.00	(2.7, 2.9, 3.0)	(6.2, 7.2, 8.0)		
	4	38.6	1.00	(0.7, 0.7, 0.8)	(4.7, 5.3, 6.1)		
	5	40.7	1.00	(0.1, 0.1, 0.1)	(1.5, 2.0, 2.9)		
	6	55.6	1.00	1.6	(10.1, 11.0, 12.7)		
	7	120.5	1.00	(21.2, 22.8, 24.5)	(63.4, 78.0, 90.9)		
080805	1	1.5	1.00	(5.9, 6.5, 7.2)	(37.2, 42.5, 47.4)	1.505	677.0/251
	2	124.4	1.00	51.9	(57.4, 65.7, 75.3)		

Note. T_{pk}, $T_{\rm rise}$ and T_f are in second. A single value indicates a parameter which was fixed during fitting. The 90 per cent range and the best-fitting value are given for parameters which were allowed to float in the fitting. The redshifts were taken from Prochaska et al. (2005), Bloom, Perley & Chen (2006), Fynbo et al. (2007), Jakobsson et al. (2008), Thoene, Perley & Bloom (2007) and Jakobsson et al. (2006).

The combination of the pulse profile function $P(t, T_f, T_{\rm rise})$ and the time-dependent blueshift of the spectral profile $B(z)$ governed by the index d produce the rise and fall of the pulse. If $d = -1$, the temporal decay index of the photon count rate after $t = T - T_{\rm ej} = T_f$ at frequency ν is $\alpha_\nu = 2 + \beta_\nu$ where β_ν is the spectral index of the Band function at that frequency. Thus, this formulation embodies the well-known closure relation between the temporal and spectral indices from the HLE. In the original formulation of Genet & Granot (2009), the datum for the characteristic energy of the Band function was E_0 at time $T_{\rm ej} + T_0$. However, we have

Table 2. Spectral parameters for the fitted pulses.

GRB	Pulse	F_f	E_f	b_1	$b_1 - b_2$	$E_{\rm peak}$	L_f
050724	1	(65.5, 75.9,173.1)	1000.	(−0.94,−0.71,−0.66)	1.00	289. ± 142.	$(2.13 \pm 1.51)10^{50}$
	2	(1.72, 1.85, 2.02)	(2.18, 2.48, 2.74)	(1.02, 1.11, 1.26)	3.00	5.2 ± 0.7	$(3.72 \pm 0.30)10^{48}$
	3	(0.00052,0.00068,0.00084)	186.	(−1.00,−0.68,−0.34)	1.00		$(1.47 \pm 0.35)10^{45}$
050814	1	(6.6, 10.5, 23.8)	1000.	(−1.03,−0.79,−0.54)	1.00		$(4.16 \pm 3.42)10^{52}$
	2	(4.32, 5.44, 6.73)	637.	(−1.25,−1.19,−1.13)	1.00		$(2.05 \pm 0.46)10^{52}$
051001	1	(2.66, 3.19, 5.48)	540.	(−0.96,−0.80,−0.60)	1.00	108. ± 98.	
	2	(4.73, 5.52, 6.34)	(10., 12., 15.)	(0.15, 0.22, 0.30)	1.00	15. ± 3.	
060211A	1	(4.03, 5.12, 6.72)	1000.	(−1.12,−1.03,−0.96)	1.00		
	2	(3.67, 4.80, 6.30)	240.	(−0.73,−0.66,−0.58)	1.00	82. ± 19.	
060814	1	(49.8, 56.3, 63.9)	1000.	(−0.45,−0.41,−0.38)	1.00	589. ± 34.	$(4.01 \pm 0.51)10^{51}$
	2	(79.0, 92.1,113.6)	694.	(−0.48,−0.42,−0.35)	1.00	403. ± 43.	$(5.70 \pm 1.07)10^{51}$
	3	(38.1, 42.4, 47.5)	(146., 183., 235.)	(−0.41,−0.37,−0.32)	1.00	116. ± 29.	$(2.00 \pm 0.22)10^{51}$
	4	(6.86, 8.45, 9.97)	(0., 167., 329.)	(−0.35,−0.30,−0.27)	1.00	117. ± 116.	$(4.19 \pm 0.77)10^{50}$
	5	(0.525,0.570,0.615)	120.	(−1.55,−1.43,−1.34)	1.00		$(1.46 \pm 0.12)10^{49}$
061110A	1	(6.14, 8.67,12.82)	1000.	(−0.90,−0.79,−0.70)	1.00	206. ± 100.	$(2.90 \pm 1.12)10^{50}$
	2	(0.494,0.517,0.541)	87.	(−2.78,−2.64,−2.52)	1.00		$(4.82 \pm 0.22)10^{48}$
061121	1	(22.9, 29.3, 48.2)	685.	(−0.70,−0.63,−0.64)	1.00	251. ± 20.	$(4.26 \pm 1.84)10^{51}$
	2	(94., 112., 133.)	625.	(−0.44,−0.40,−0.35)	1.00	377. ± 27.	$(2.08 \pm 0.36)10^{52}$
	3	(130., 158., 195.)	563.	(−0.37,−0.32,−0.27)	1.00	381. ± 30.	$(3.10 \pm 0.63)10^{52}$
	4	(158., 176., 203.)	374.	(−0.27,−0.23,−0.20)	1.00	288. ± 13.	$(3.39 \pm 0.44)10^{52}$
	5	(438., 519., 605.)	698.	(0.19, 0.22, 0.26)	1.00	849. ± 23.	$(2.64 \pm 0.42)10^{53}$
	6	(2.03, 2.33, 3.75)	50.	(−1.93,−1.64,−1.40)	1.00		$(1.89 \pm 0.70)10^{50}$
061222A	1	(7.39, 9.36,43.08)	854.	(−0.92,−0.53,−0.11)	1.00	398. ± 344.	
	2	(23.5, 43.2, 81.8)	1000.	(−0.79,−0.62,−0.45)	1.00	380. ± 166.	
	3	(17.2, 18.7, 27.9)	1000.	(−0.84,−0.72,−0.66)	1.00	279. ± 90.	
	4	(15.7, 21.7, 30.0)	1000.	(−0.77,−0.68,−0.59)	1.00	324. ± 88.	
	5	(70.9, 75.2, 96.3)	197.	(0.10, 0.17, 0.25)	1.00	230. ± 15.	
	6	(113., 165., 186.)	573.	(−0.13,−0.03, 0.00)	1.00	554. ± 38.	
	7	(37.6, 44.2,110.0)	466.	(−0.47,−0.18, 0.17)	1.00	384. ± 149.	
	8	(0.484,0.564,0.698)	(1.09, 4.89, 8.42)	(−1.65,−1.63,−0.88)	1.00		
070420	1	(15.9, 37.9, 60.2)	900.	(−0.29,−0.07, 0.18)	1.00	837. ± 211.	
	2	(39.0, 44.4, 65.4)	1000.	(−0.36,−0.18,−0.02)	1.00	822. ± 170.	
	3	(105., 133., 184.)	1000.	(−0.37,−0.29,−0.20)	1.00	710. ± 84.	
	4	(61.4, 85.3,126.9)	1000.	(−2.06,−1.92,−1.83)	1.00		
070621	1	(40.1, 43.8, 77.3)	765.	(−0.45,−0.31,−0.15)	1.00	530. ± 115.	
	2	(19.9, 25.2, 41.1)	1000.	(−1.08,−0.68,−0.68)	1.00	316. ± 201.	
	3	(21.2, 28.4,136.4)	1000.	(−1.25,−1.00,−0.85)	1.00		
	4	(57.3, 70.1,117.3)	1000.	(−1.51,−1.38,−1.20)	1.00		
	5	(25.7, 31.6, 92.9)	731.	(−0.53,−0.21,−0.15)	1.00	578. ± 140.	
	6	(0.482,0.536,0.594)	387.	(−1.78,−1.62,−1.47)	1.00		
080229A	1	(54.9, 61.2,123.5)	1000.	(−0.58,−0.38,−0.17)	1.00	615. ± 204.	
	2	(11.4, 70.0,244.3)	660.	(−1.36,−0.96,−0.87)	1.00		
	3	(115., 160., 230.)	503.	(−0.91,−0.81,−0.74)	1.00	97. ± 44.	
	4	(327., 560., 911.)	420.	(−1.51,−1.36,−1.20)	1.00		
	5	(44., 179.,1056.)	517.	(−1.72,−0.98,−0.94)	1.00		
	6	(143., 260., 715.)	1000.	(−2.24,−2.05,−1.94)	1.00		
	7	(0.653,0.761,0.979)	(0.80, 2.52, 5.08)	(−2.22,−1.96,−1.67)	1.00		
080805	1	(2.6, 15.1, 25.4)	(48., 60., 86.)	(0.50, 0.80, 0.81)	2.50	108. ± 36.	$(2.86 \pm 2.15)10^{51}$
	2	(0.379,0.483,0.528)	(1.14, 1.48, 1.61)	(0.77, 1.05, 1.06)	2.50	3.0 ± 0.5	$(7.46 \pm 1.15)10^{49}$

Note. F_f 10^{-8} erg cm^{-2} s^{-1} over the energy band 0.3–350 keV is the flux at peak, E_f keV is the cut-off energy at peak, $E_{\rm peak} = (b_1 + 1)E_f$ keV is the energy peak of the $\nu F(\nu)$ spectrum and L_f erg s^{-1} is the isotropic peak luminosity. A single value indicates a parameter which was fixed during fitting. The 90 per cent range and the best-fitting value are given for parameters which were allowed to float in the fitting.

chosen to use E_f at time T_{pk} because this time marks the maximum of the emission when we get the best measurement and estimate of the spectral profile.

Previous authors have attempted to model the prompt pulses of GRBs (e.g. Norris et al. 2005). The empirical pulse profile employed incorporated an exponential rise followed by an exponential decay and the profile was fitted independently to each energy band to map any changes of the time constants as a function of energy. The pulse profile used for the current work is physically motivated and based on a simple but reasonably realistic model. The rise and

Table 3. Comparison of $E_{\rm peak}$ keV at time T_{pk} derived in the present work with average values, $\bar{E}_{\rm peak}$ keV, derived for a Band function using combined *Swift*/BAT and *Suzaku* WAM data (Krimm et al. 2009) and cut-off power-law fits to *Konus–Wind* data (Page et al. 2007).

GRB	Pulse	T_{pk} (s)	$E_{\rm peak}$ (keV)	Interval (s)	$\bar{E}_{\rm peak}$ (keV)
060814	1	10.1	589 ± 34	−11.75–10.75	365^{+119}_{-95}
	2	16.5	403 ± 43	10.75-30.75	350^{+136}_{-100}
061121	2	61.9	377 ± 27	61.876–70.324	478^{+158}_{-99}
	3	68.6	381 ± 30		
	4	73.7	288 ± 13	70.324–75.158	608^{+87}_{-71}
	5	75.0	849 ± 23	75.188–83.380	621^{+282}_{-159}
061222A	3	60.0	279 ± 90	34.29–89.29	415^{+210}_{-159}
	4	73.8	324 ± 88		
	5	83.0	230 ± 15	75.29–99.79	248^{+163}_{-68}
	6	87.0	554 ± 38	80.29–89.79	299^{+122}_{-80}
	7	90.0	384 ± 149		

Note. The errors and error ranges quoted are 90 per cent confidence. Both T_{pk} and interval are time since BAT trigger.

fall of the pulse are modelled by power laws and the spectral behaviour/evolution is incorporated into the Doppler shift of the spectral profile as a function of time. The resulting temporal–spectral profile is fitted simultaneously to all energy bands.

The prompt emission of a typical burst comprises several pulses and although the spectral–temporal evolution of each pulse in the model is governed by the same simple formulation the evolution of a linear superposition of pulses can be complex. Each pulse can have a different spectrum (E_f, b_1 and b_2), different time-scales ($T_{\rm rise}$ and T_f) and different brightness ($B_{\rm norm}$). The current model imposes no restriction on the order or magnitude of the time-scales or spectral parameters in the pulse sequence and therefore the characteristic energy of the combined spectrum can increase or decrease with time in a complicated fashion.

3 MODEL FITTING

We have attempted to fit the complete *Swift* BAT and XRT light curves of the selected sample of 12 GRBs using the above model for the prompt pulses. An afterglow component fit to the plateau and final decay of the XRT light curve as specified by Willingale et al. (2007) was also included so that the transition from the initial decay from the prompt into the plateau phase of the afterglow was modelled in a consistent way. The standard energy bands were used for the BAT (15–25, 25–50, 50–100 and 100–350 keV) and XRT (0.3–1.5 keV and 1.5–10 keV). XSPEC (Arnaud 1996) version 12.4.0 was used to calculate the expected count rates in these energy bands from the prompt pulse and afterglow components. The number of individual count rate predictions required to find a best-fitting model is very large, $\sim 500\,000$, for each pulse or afterglow component. Therefore, using XSPEC directly for each evaluation would have been prohibitively time consuming (taking many hours to run on a desktop PC). Instead, XSPEC was used to generate a lookup table of count rates over a 3D grid of spectral parameters for the Band function, $[b_1, b_1 - b_2$ and $\log_{10}(E_c)]$, and the fitting was done by linear interpolation of the predicted count rates within the lookup table. A look-up table of $20 \times 20 \times 20$ samples typically takes 20 min to generate but the fits can then be done in a few seconds. It was found that the Band function model in XSPEC, Grbm, was unable to generate spectra with $E_c < 1.0$ keV because there is a hard limit set in the code. Unfortunately, late-time spectra from the pulse model above can easily reach such low values of characteristic energy so we had to create a local Band function model for XSPEC without this restriction.

The count rates in the low-energy XRT band are sensitive to the assumed absorption column density. Fixed values of both the Galactic and instrinsic column density were included in the spectral model run in XSPEC using WABS (and ZWABS if the redshift was known). These column density values were determined separately from spectral fits to the XRT data. For the GRBs in the sample, the early XRT data are dominated by prompt continuum which may not be a simple power law and the intrinsic column density determined using these data might be compromised. We used late-time data when available and for some bursts with larger intrinsic column density we tried running the fits with different intrinsic column density values to see if this influenced the results. The systematic errors introduced by uncertainties in the column densities are smaller than the 90 per cent range produced by the fitting so the fits remain essentially the same.

It was easy to make an initial guess for T_{pk} and $T_{\rm rise}$ for each pulse. Using this guess, a fit was then done letting T_{pk}, $T_{\rm rise}$ and T_f vary to find a reasonable fit to the pulse profile and a best-fitting value for T_{pk}. This value of T_{pk} was then fixed in all subsequent fitting to find the best-fitting values of both the spectral and temporal parameters. In some cases, the rise of the pulse is not well constrained by the data and for these bursts $T_{\rm rise}$ was fixed. There is in fact some redundancy between the $T_{\rm rise}$ and a parameters. A fast rise can be achieved using $a = 1$ and small $T_{\rm rise}$ but can also be fitted using a larger $T_{\rm rise}$ and $a > 1$. For most pulses, the number and quality of the data points over the rise are such that it is not possible to fit these two parameters simultaneously. For fast cooling, we expect $a + d = 0$ and in order to reduce the number of free parameters we included this constraint in the fitting. In most cases, we fixed $a = 1$ and hence $d = -1$.

The initial values assumed for E_f and $b_1 - b_2$ were 1000 keV and 1, respectively. This specifies a transition to the high-energy power law at $E = (b_1 - b_2)E_f$=1000 keV. The $b_1 - b_2$ values derived for bursts observed with *BATSE* have a considerable spread (Band et al. 1993) but $b_1 - b_2 = 1$ is typical. E_f was allowed to float to a lower energy to find the best fit. In a few cases, the χ^2 was very insensitive to E_f and the best-fitting energy exceeded 1000 keV. For these pulses, E_f was fixed at 1000 keV. There is some

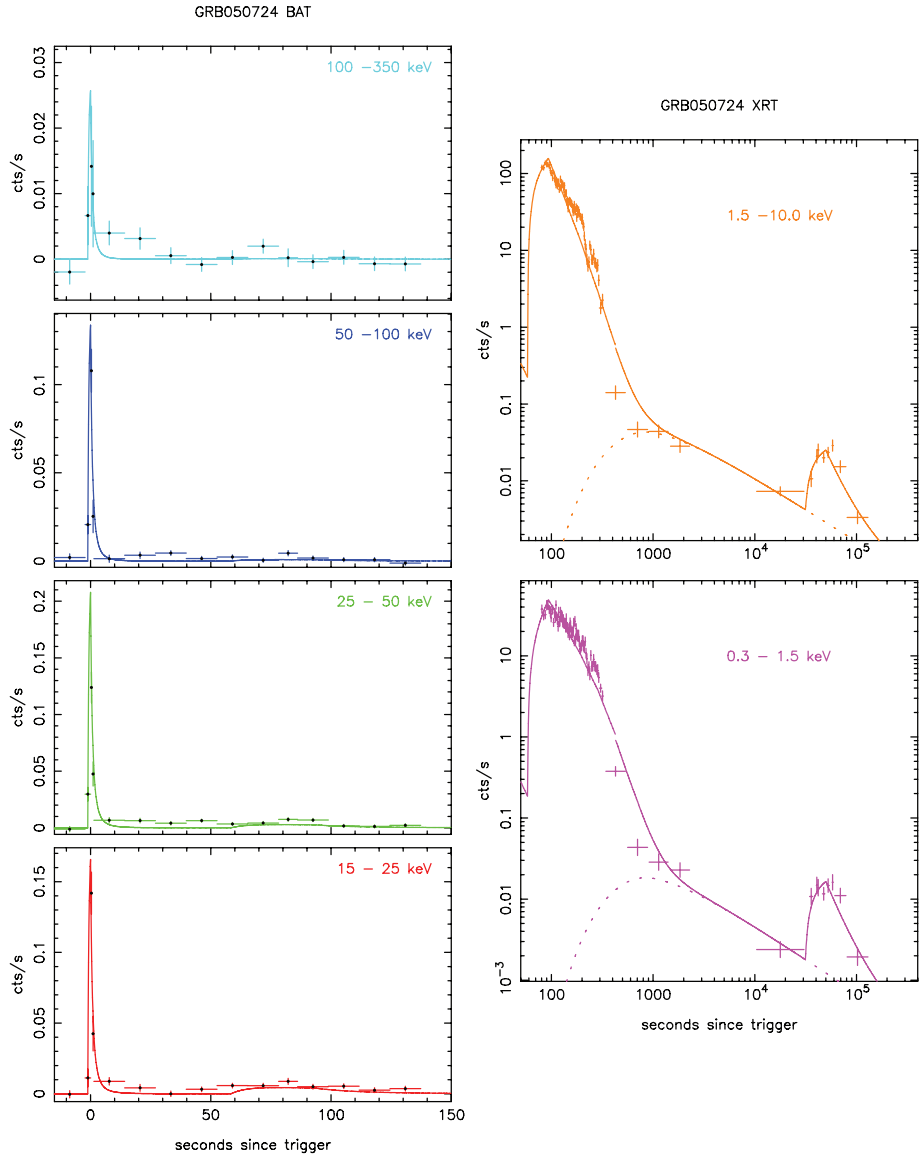

Figure 2. GRB050724.

degeneracy/coupling between E_f and the spectral index b_1, and for most pulses the errors are too large to provide independent estimates of these two parameters which determine the spectral shape. In all cases, we estimated the error range for b_1 but we were only able to estimate an error range of E_f for a few pulses. In subsequent analysis, we combine E_f and b_1 to estimate the $E_{\rm peak}$ value and use this single parameter to characterize the hardness of the spectrum. None of the fits is able to really constrain $b_1 - b_2$ because the BAT response does not extend to high enough energies and the total count available from individual pulses is usually considerably less than the total fluence. However, three soft pulses, pulse 2 in 050724 and both the pulses in 080805, gave a significantly better fit using a cut-off power law without a high-energy tail ($b_1 - b_2 \rightarrow \infty$). For these pulses, we investigated how low $b_1 - b_2$ in the Band function could be set before the fit was significantly worse than the cut-off power law. In these cases, the fixed $b_1 - b_2$ used for the fit is effectively an estimate of the lower limit for the change in index into the high-energy tail of the Band function.

The fitting was performed using a search for minimum χ^2 and the resulting minimum χ^2 found along with the number of degrees of freedom (d.o.f.) are listed in Table 1. The product $F_f T_f^{2+b_1}$ for each pulse determines the relative contribution it will make to the decaying tail of the prompt emission and all the major pulses visible in the light curves were included in the modelling. Some faint pulses visible in the data were not included in the model because they were too faint to contribute significantly to the RDP. There are features in all the light curves which are not well fit by the model and the final χ^2_ν values are not statistically acceptable. Other ways in which the data do not conform to the model can be seen in the plots of the fits provided below and will be discussed later.

Some theoretical/physical constraints were ignored. Pulses were fitted independently with no attempt to introduce coupling between their parameters. So, it is possible that a slow pulse could start before a fast pulse but peak after the same fast pulse. In the simple version of the theoretical model with constant Γ this is clearly not physically possible. We return to this point in the Discussion.

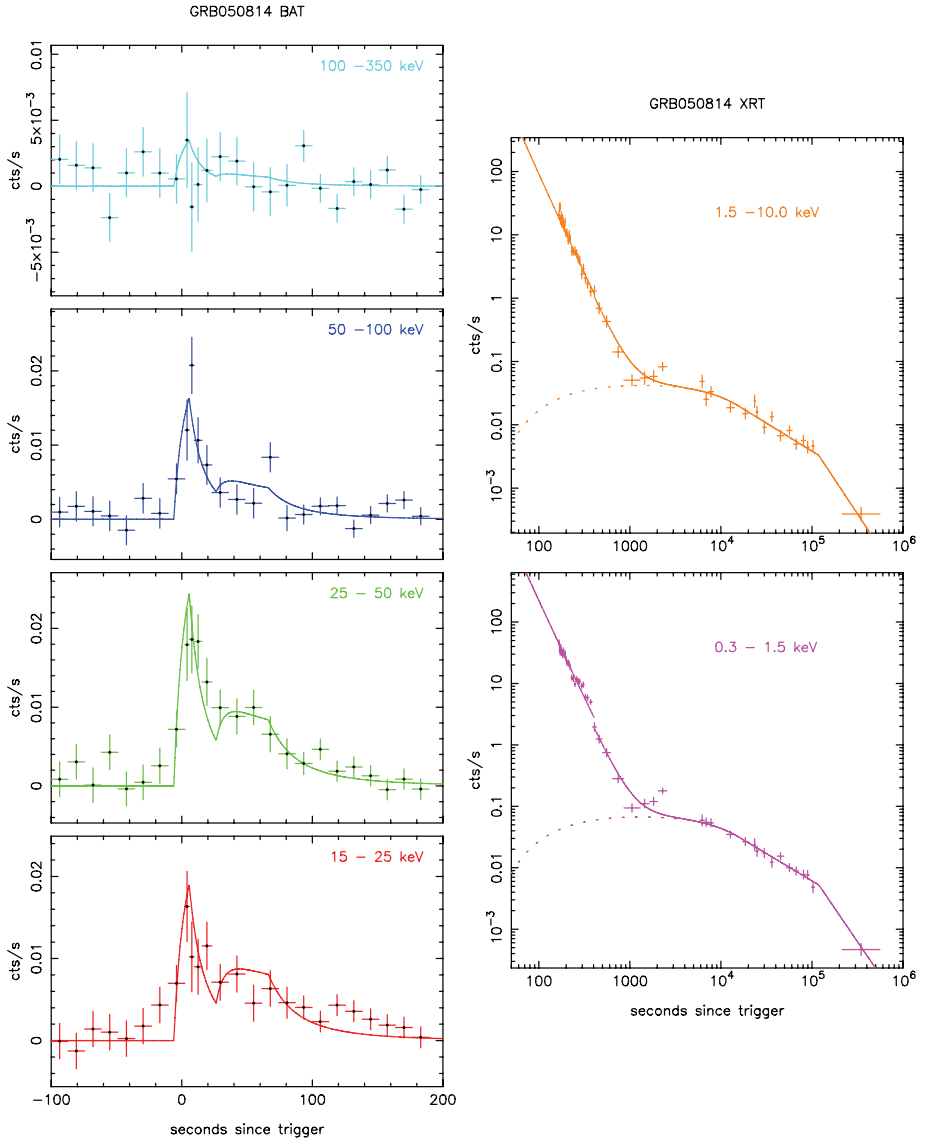

Figure 3. GRB050814.

4 FITTING RESULTS

Tables 1 and 2 list the fitted parameter values obtained. The sequence of pulses used for each burst is numbered in temporal order. When a parameter was allowed to vary, the 90 per cent confidence range is given in parentheses with the best-fitting value in the centre. In Table 1, T_{pk} seconds is the time since the trigger of the start of the final decay of the pulse at the elapsed time T_f seconds after ejection. This is usually the peak of the pulse but can be a little later. The last column provides the redshift values where available. In Table 2, b_1 is the low spectral index of the Band function (i.e. $b_1 = \alpha + 1$ where α is the low photon index in the original formulation of the Band function) and $b_1 - b_2$ is the difference between the low and high spectral indices of the Band function. F_f is the flux in units of 10^{-8} erg cm^{-2} s^{-1} over the energy band 0.3–350 keV at time T_{pk} and E_f keV is the characteristic energy of the Band function at that time. The peak energy of the $\nu F(\nu)$ spectrum at time T_{pk} is given by $E_{\rm peak} = (b_1 + 1)E_f$ and of course this peak energy evolves with time in the same way as the characteristic energy. If $b_1 < -1$ then there is no positive peak energy and for these very soft pulses $E_{\rm peak}$ is probably below the XRT energy band. For pulses where the 90 per cent range of b_1 encompasses -1 we have not listed an $E_{\rm peak}$ value. Note, we quote the flux over the combined XRT and BAT energy band because all the fits incorporate data from both the instruments. The last column of Table 2, L_f, is the isotropic luminosity erg s^{-1} at time T_{pk} over the bolometric energy band 1–10 000 keV. This was estimated from the flux F_f using the redshift and assuming a cosmology with $H_0 = 71$ km s^{-1} Mpc^{-1}, $\Omega = 0.27$ and $\Lambda = 0.73$ to calculate the luminosity distance $d_{\rm L}$.

We want to stress that the fitted $E_{\rm peak}$ values listed in Table 2 are the value of this spectral parameter at a specific time, T_{pk} seconds after the BAT trigger. We are able to obtain such values from a Band function fit because we are fitting both the spectral and the temporal profiles of the pulse simultaneously. During a typical pulse the peak energy will range from a factor of ∼1.5, greater than this value, at the start of the rise, to a factor ∼0.2, smaller than this value, when the tail of the pulse disappears into the noise or is obscured by a subsequent pulse. The average pulse spectrum expected from

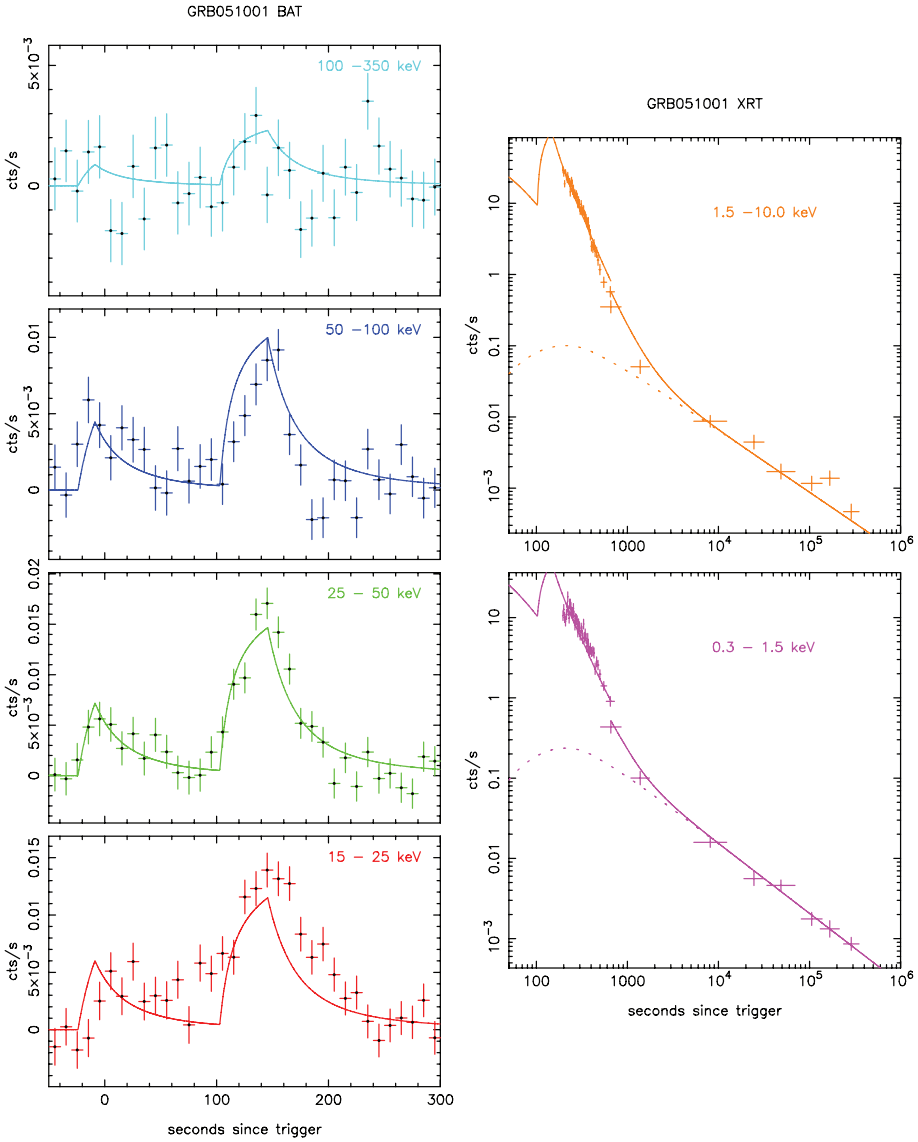

Figure 4. GRB051001.

the model is a weighted sum or convolution of a series of Band profiles. If the pulse spectrum summed over the main peak were fitted with a Band function, we would get an average peak energy values, $\bar{E}_{\rm peak}$, which would be similar to but not the same as the $E_{\rm peak}$ values derived by the current technique. Actually, most pulses are too weak to provide sufficient statistics to fit a Band function to the average pulse spectrum seen in the *Swift* BAT. However, Krimm et al. (2009) were able to fit spectra over relatively small time intervals using a combination of *Swift* BAT and *Suzaku* Wide-band All-Sky Monitor (WAM) data and Page et al. (2007) provide a listing of $E_{\rm peak}$ values derived for short time intervals of 061121 from cut-off power-law fits to *Konus–Wind* data. In Table 3, we list a small subset of the peak energy results which are common between the present work and these studies. The $\bar{E}_{\rm peak}$ are indeed similar to our $E_{\rm peak}$ values although they tend to be a little lower because the average pulse spectrum is a little softer than that at the peak. When a soft pulse is followed by a hard pulse as is the case for pulses 4 and 5 of 061121 then the $\bar{E}_{\rm peak}$ value increases as expected. The second time interval for 061121 contains pulse 4 ($E_{\rm peak} = 288$) and the start of pulse 5 ($E_{\rm peak} = 849$) so the $\bar{E}_{\rm peak} = 608$ is a blend of the two. The third time interval for 061121 contains just pulse 5 and is a little harder with $\bar{E}_{\rm peak} = 621$ but not as hard as the peak value for pulse 5.

The fits for all 12 bursts included are illustrated by the Figs 2 through 13 in date order. The BAT count rates are per detector. The observed total count rate is much larger than these values and depends on the position of the burst within the BAT field of view. The sections below provide a brief commentary on all the fits including a description of the features which are dominating the $\Delta\chi$ distribution in each case. We have studied the residuals in detail to see if it likely that the fitted parameters and the estimated confidence ranges are compromised by the rather high reduced Chi-squared values. In three cases, the quoted error range may be too small because of systematic problems with the fitting. These are the second pulse in 050724 in the 15–25 keV band, the first pulse in 060211A in the 50–100 keV band and the first pulse of 080805 in the 15–25 keV

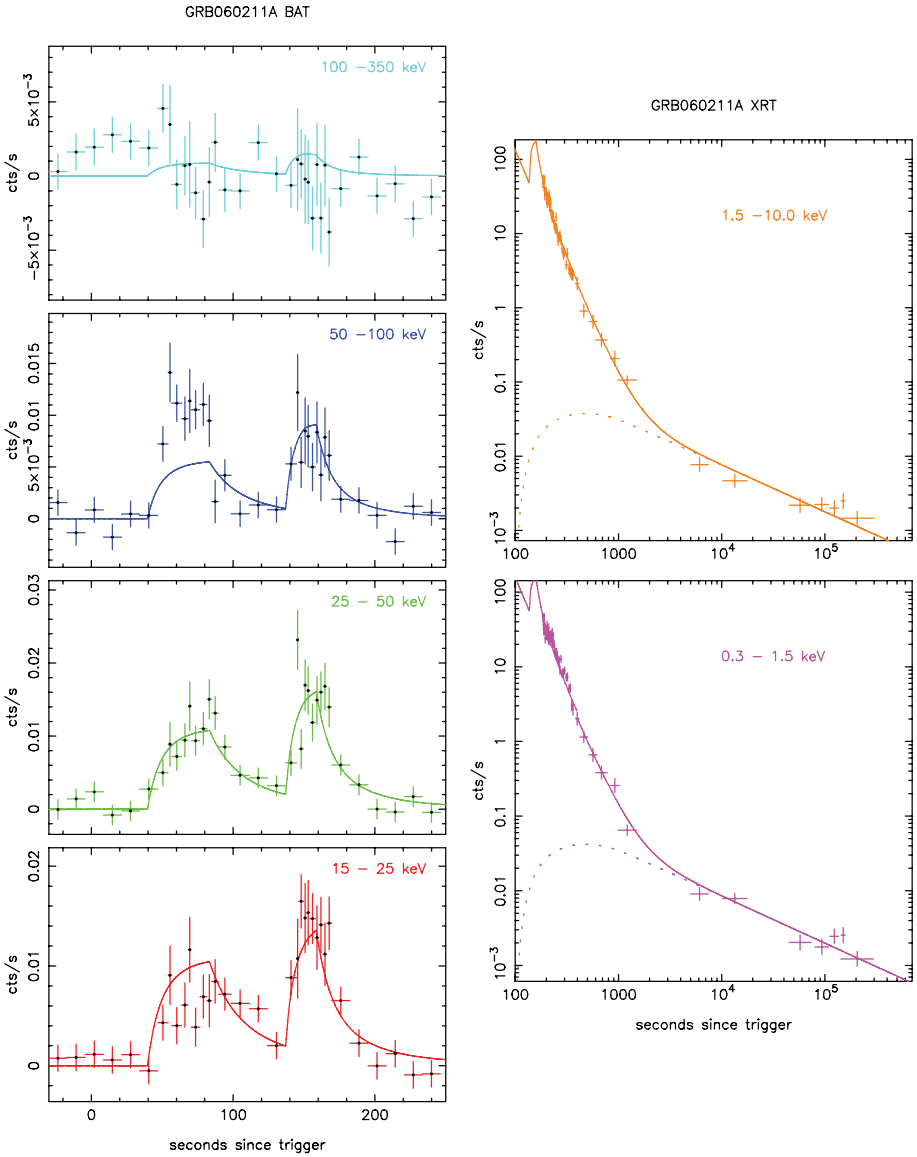

Figure 5. GRB060211A.

band. In these pulses, the observed flux is systematically higher than the model in the quoted band over a significant fraction of the peak.

4.1 GRB050724

This is an example of a short burst with an extended emission tail that is just visible in the *Swift* BAT over a prolonged period such that $T_{90} = 96$ s. This extended emission is seen as a very broad weak rise in the BAT count rate peaking at about 80 s and as a very early bright flare in the XRT. This is fitted by the second pulse although it is not possible to find a Band function spectrum which fits the BAT and XRT profiles exactly. The fit shown in Fig. 2 has the highest reduced Chi-squared value of any of the fits. The model is a little too low over most of the BAT 15–25 keV band and does not quite match the shape of the tail of the RDP in the XRT 0.3–1.5 keV band. For this essentially short burst, the RDP observed is entirely due to the extended emission and not the initial short pulse. Coincidentally, this bright, soft second pulse gave rise to an expanding dust-scattered X-ray halo around this GRB as reported by Vaughan et al. (2006). This burst also has a late flare seen in the XRT which is included as the third fitted pulse with $T_{pk} = 50\,000$ s and $T_f = 43\,000 \pm 11\,000$ s.

4.2 GRB050814

GRB050814 comprises a fast rise exponential decay (FRED) pulse followed by a weaker second pulse the decay of which was tracked well by the XRT. The fitted model cannot match the short hard peak of the pulse (seen in the BAT 50–100 keV band) which decays rapidly combined with the softer pulse which decays more slowly. The pulse profile is not well fit in the BAT 15–25 keV band. The rapid decay of the pulse is well fit by the predicted HLE of the model in both XRT energy bands except at the transition into the start of the afterglow plateau. This is a good example where the

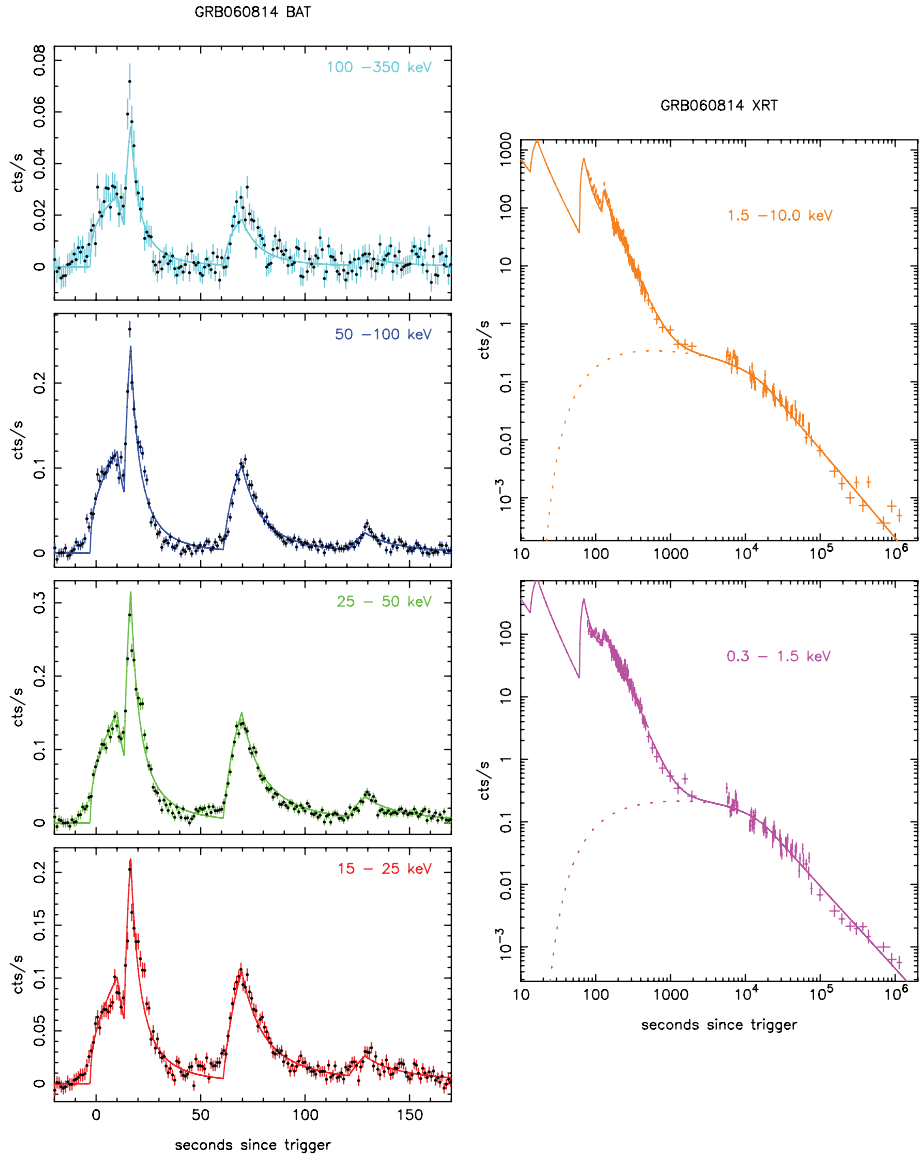

Figure 6. GRB060814.

data suggest a slower decline before 100 s (in the BAT 15–25 keV band) but a faster decline later, in the XRT bands.

4.3 GRB051001

A rather weak burst modelled by two pulses. The second pulse is seen in both the BAT and the XRT and the best fit is achieved using an $E_f = 15 \pm 3$ keV, which is in between the XRT and BAT band passes. As with other bursts, the profile is not a good fit in the lowest BAT band 15–25 keV. There is also evidence for curvature of the decay of the second pulse in the XRT bands which is not matched by the model.

4.4 GRB060211A

This is a rather faint burst seen in the BAT which is reasonably well represented by two pulses except that the pulse profiles in the 50–100 keV band have rather flat tops with a sharp drop at the end which is not emulated by the model. The fit for the first pulse in the 50–100 keV band is particularly poor and it looks as if the spectrum should be harder for this pulse. However, if the spectral index is made smaller to accommodate this the decay of the pulse is too shallow. i.e. it is not possible to satisfy the closure between the spectral and temporal indices for this pulse. The RDP seen in the XRT is very well matched by the model.

4.5 GRB060814

GRB060814 was a bright burst consisting of three well-separated main pulses in the BAT seen with excellent statistics. The best fit to the second and third pulse does not quite capture the narrow hard peak seen in the BAT 100–350 keV band. The detailed shape of the decay of the second pulse is not well fitted and the residuals on this decay contribute significantly to the Chi-squared value. We tried varying the index a, but this did not improve the fit. We also tried lifting the constraint $a + d = 0$ and fitting a and d independently, but this did not improve things either. The fourth pulse is seen in both the BAT and the XRT and it proved impossible to fit these data

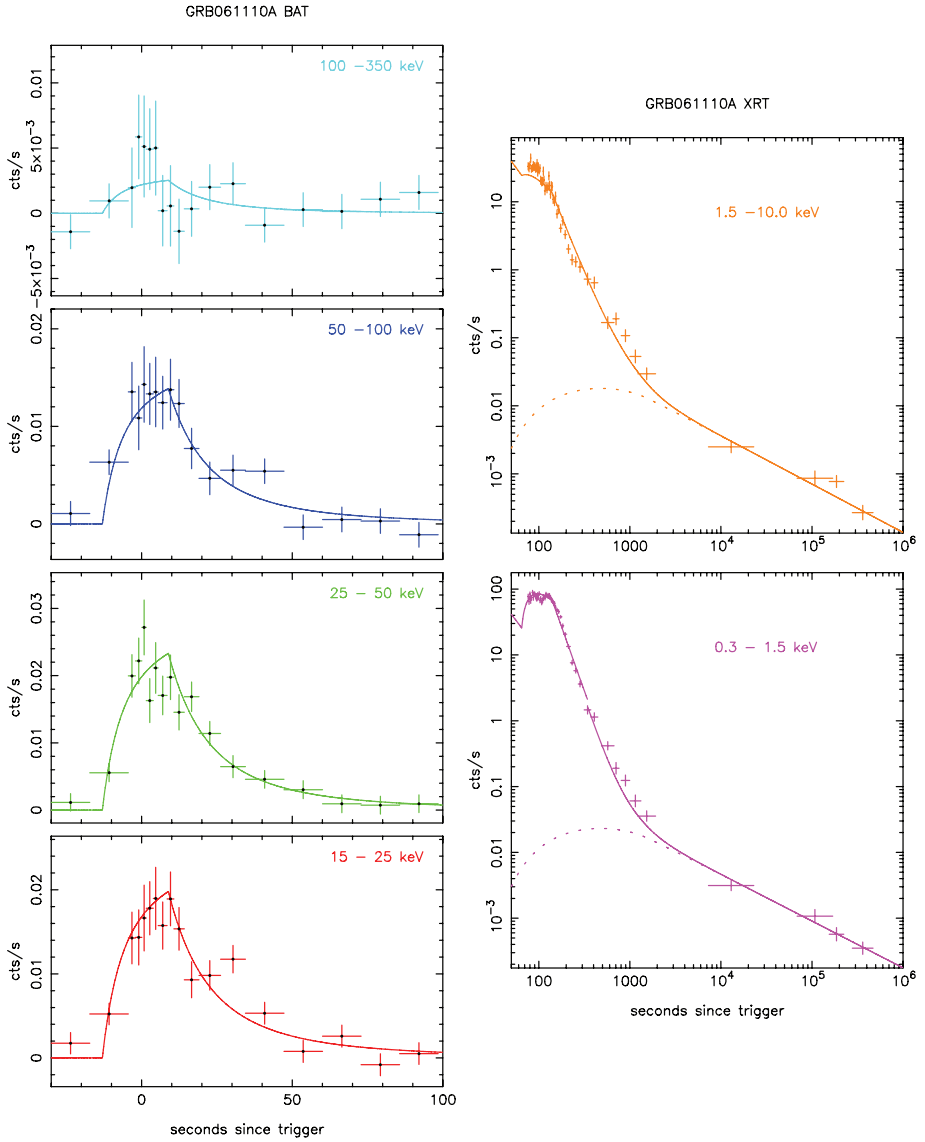

Figure 7. GRB061110A.

with a single pulse. If we fit to the BAT only then $T_f = 28$ s and the decay falls well below the XRT data for $t > 150$ s. Fitting both the BAT and XRT gives $T_f = 113$ s but the peaks in the BAT are missing and the fit is dominated by the XRT because there are many more data points from the low-energy instrument. It is not possible to find a spectrum which can produce both the fast, narrow hard pulse and the wider soft decay.

The fit shown in Fig. 5 consists of a fourth hard pulse which fits the peak seen in the BAT and a slightly later peaking soft pulse which fits the decay seen in the XRT. If we calculate the ejection times $T_{\rm ej} = T_{pk} - T_f$ for the fourth and fifth pulses, we get 92 s and −102 s, respectively. Under the simple assumptions of the model, this is unphysical since the fifth pulse is launched before the fourth pulse (and indeed before the first and second pulses!) but the peak is seen after the fourth pulse.

4.6 GRB061110A

This burst comprises a single FRED pulse seen in the BAT followed by a soft pulse seen only in the XRT. The pulse profiles and the decay into the afterglow are both well fit by a simple two pulse model. There is a slight mismatch around the transition from the rapid decay into the afterglow.

4.7 GRB061121

GRB061121 triggered on a well-defined precursor which was separated from the main body of the burst by about a minute. This gave *Swift* time to slew on to source and so the XRT was able to capture several pulses of the prompt emission alongside the BAT. The source exhibited detailed spectral evolution as described by Page et al. (2007). The current model includes six pulses, three of which were seen in both the BAT and XRT. Because the statistics are good, the model is unable to reproduce all the features in the data but the overall fit is reasonable. In particular, the cusps of the peaks of pulses 3–5 have rather large residuals although they are difficult to see on the plot in 8. The fifth and brightest pulse is of particular note. The decay from the narrow peak is very rapid but the spectrum is hard, $b_1 = 0.22 \pm 0.04$, and close to a power law over the full BAT and XRT range. It is impossible to fit this decay

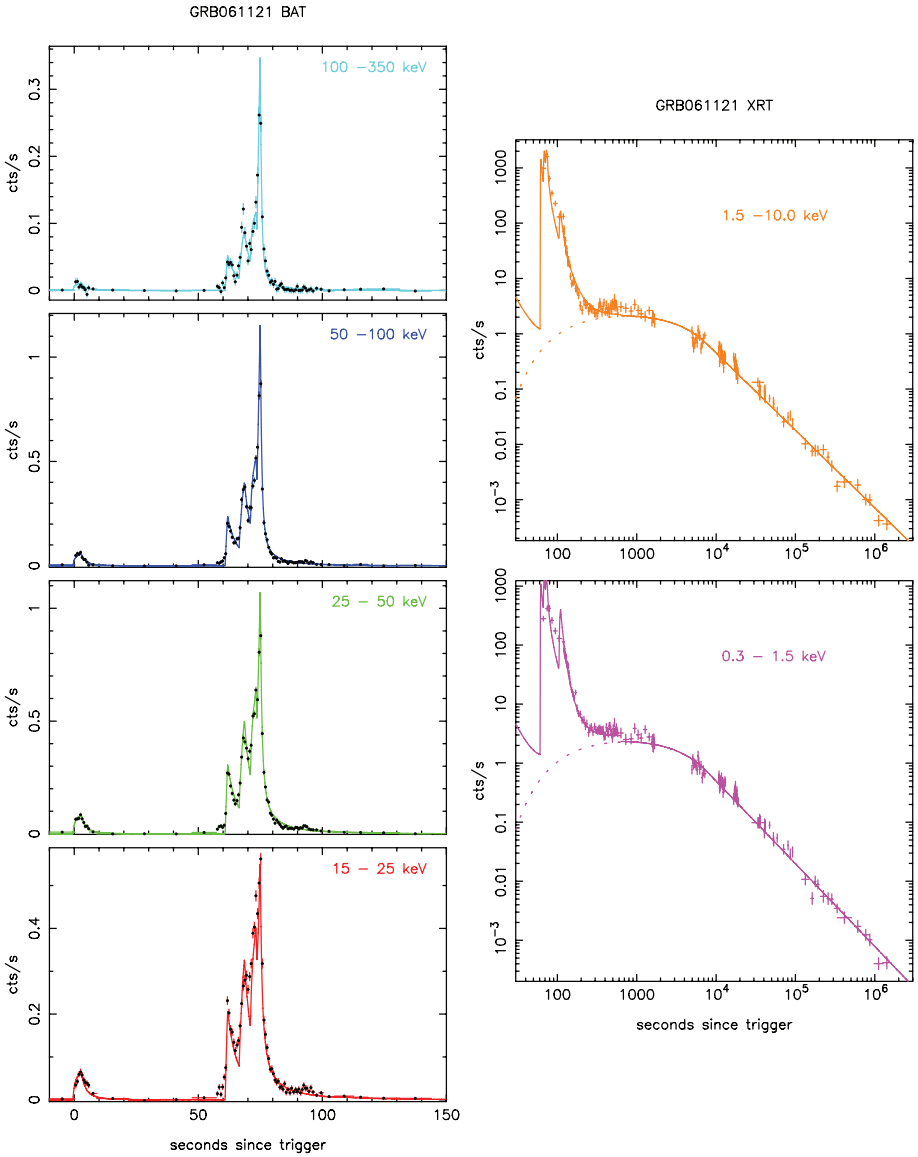

Figure 8. GRB061121.

using the standard model index $a = 1.0$. The fit shown in Fig. 8 uses $a = 2.4$ (and hence $d = -2.4$). A sixth pulse seen chiefly in the XRT interrupts the decay but the overall fit of the HLE component from the pulses using this large index value is good.

4.8 GRB061222A

A total of eight pulses was used to model this bright burst and there are still weak features which are not included in the model profile. The Chi-squared is dominated by the residuals at the cusps of the pulses 5–7 and the transition from the rapid decay into the afterglow.

4.9 GRB070420

The rather untidy BAT light curve of this burst has been fitted using four overlapping pulses. The rapid decay seen in the XRT 1.5–10.0 keV band is not well modelled in the latter stages before it is obscured by the plateau of the afterglow emission at ≈200 s and this makes a significant contribution to the Chi-squared but the softer decay in the XRT 0.3–1.5 keV band is well matched.

4.10 GRB070621

This burst is rather different from the others presented here because the light curve consists of a series of very similar overlapping pulses. The fit shown in Fig. 11 comprises six pulses. For all these, the width $T_{\rm rise}$ was fixed during the fitting. The BAT data are very ragged and clearly more complicated than suggested by the model. However, once again the rapid decay captured by the XRT is well fit by the model. The largest residuals occur just before the rise of the first pulse. There is clearly some emission here which is not included in the model.

4.11 GRB080229A

This burst is a good example of a sequence of well-defined pulses including a precursor 25 s before the main burst. The model is

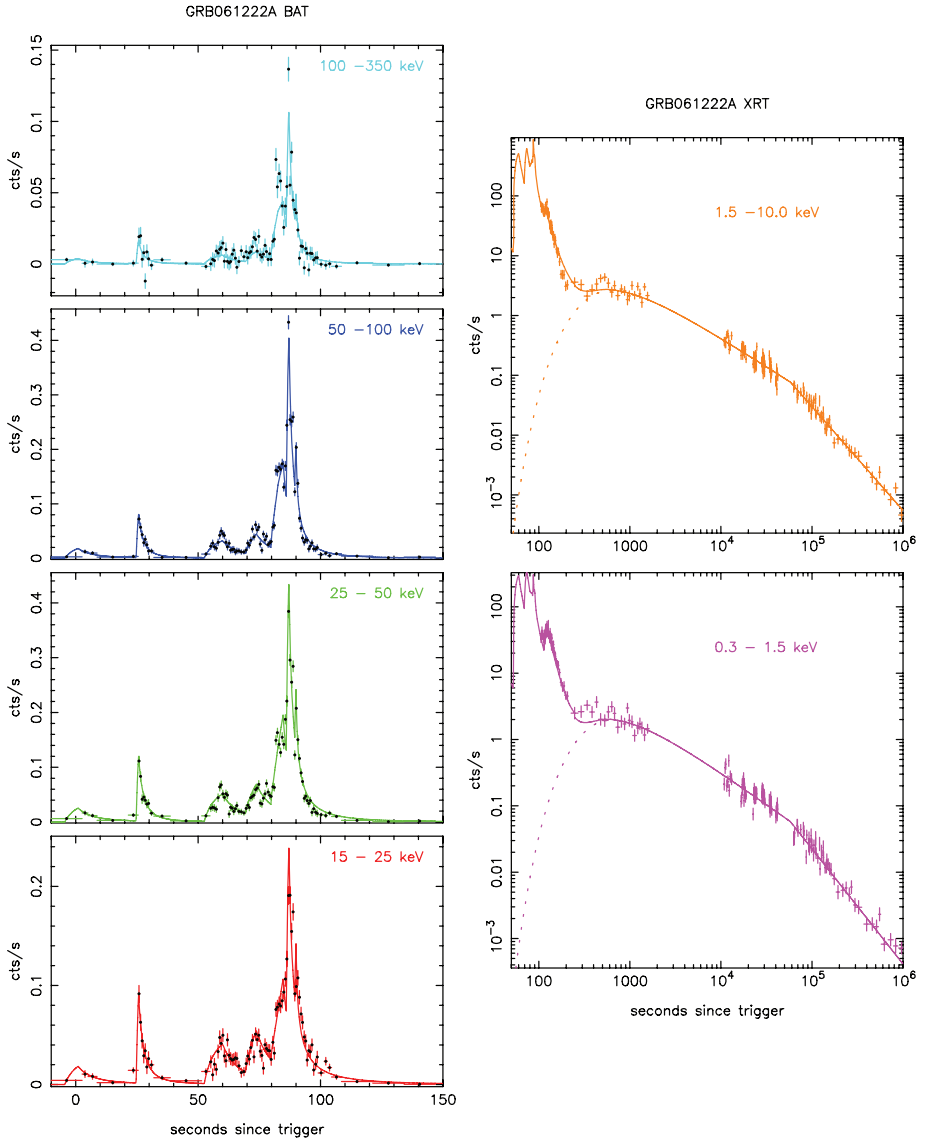

Figure 9. GRB061222A.

unable to fit the hard, narrow peak of pulses 1 (precursor) and 2–4. The residuals at the cusps of pulses 3 and 4 are particularly large.

4.12 GRB080805

This burst is well represented by just two pulses, the trigger pulse seen just in the BAT and a second soft pulse seen in the XRT. The first pulse profile is well fit in the BAT 50–100 keV band but the hard peak in the 100–350 keV band is not quite fit and there is excess emission seen in the 15–25 keV band which peaks 20 s later. We tried many different spectral profiles (other than the Band function) to try and match this behaviour without success. The soft tail of this first pulse seen at the start of the XRT observation in the 1.5–10.0 keV band is also higher than predicted. Both pulses were better fit if E_f was allowed to float and the resulting best-fitting values for this parameter are well constrained.

5 DISCUSSION

In all cases, the fit to the prompt decay from the BAT into the XRT band is reasonably good. In some cases like 050724, 051001 or 070420, there is a residual curvature in the decay which is not exactly matched by the model but in general the summation of the HLE at late times from all the pulses provides a good fit to the RDP.

There is a generic problem with fitting hard, narrow peaks in conjunction with a soft more slowly decaying tail. The fourth pulse in GRB060814 is a prime example. Here, it proved impossible to fit the peak in the BAT 50–100 keV band, which produces the decay seen in the XRT, using a single pulse. A good fit can be obtained to just the BAT data using a spectral index $b_1 = -0.56$ but this is far too hard to produce the soft tail seen in the XRT. Alternatively, the XRT profile can be fitted using $b_1 = -1.09$ but this produces no visible flux in the BAT. The fit shown in Fig. 6 includes a fifth pulse which fits the broad soft tail seen in the XRT. There is a very significant difference between the T_f values of the fourth and fifth pulses in the final fit, 38 ± 4 and 252 ± 23 s, respectively. The

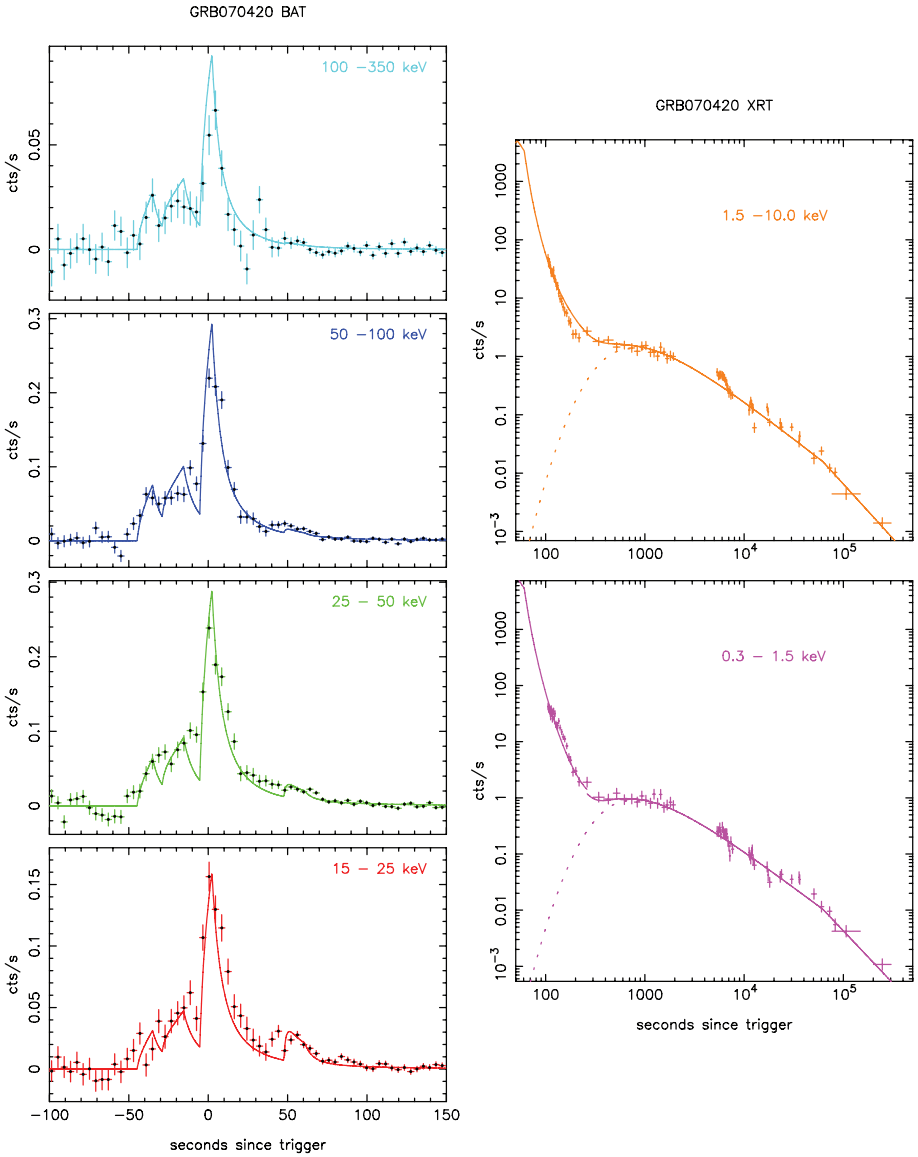

Figure 10. GRB070420.

required difference in the temporal decay times in the hard BAT and soft XRT could not be satisfied using a single spectral profile. A similar situation exists for the first pulse in GRB080805. The profile in the upper three BAT bands is reasonable but this does not fit the excess flux seen in the 15–25 keV BAT band or the start of the XRT observation in the 1.5–10 keV band before 100 s when the second pulse starts to dominate.

Despite these problems the model does accommodate an element of energy-dependent lag (Norris, Marani & Bonnell 2000) and narrowing of the pulses at high energies (Reichart et al. 2001) as illustrated in Fig. 14. The top panels shows the first pulse of 050814, a typical pulse. The characteristic energy at peak is set to 1000 keV so that the spectrum is very close to a simple power law over the BAT and XRT energy range at the peak of the pulse. The decay from the peak is a power law in each band, slightly steeper for the upper energy bands closer to the characteristic energy. The pulse profile shown in linear scaling to the right is very similar in all energy bands. For the fifth pulse in 061121 shown in the middle panels of Fig. 14, the steep decay requires $a = 2.4$ (90 per cent range 2.1–2.8), significantly higher than the standard value of $a = 1$. Because of curvature in the spectrum (the exponential factor in the Band function), the high index also has the effect of shifting the pulse peak to below T_f for the harder energy bands. The spectral lag introduced is clearly illustrated in Fig. 14. The best fits for eight of the pulses included E_f as a fitted parameter. For these pulses, there is greater spectral curvature because E_f falls within the XRT–BAT energy range and consequently the pulse profile changes between the energy bands. The bottom panels of Fig. 14 show an example of this; the first pulse in 080805. The rise of the pulse is almost identical over all energy bands but the decay is steep at high energies and shallow a low energies. The resulting pulse width is a strong function of energy although the peak itself remains at the same position. This is not a lag in the strictest sense of the term but it would appear as a lag in any analysis involving cross-correlation since the centroid of the peak clearly shifts to later times as the energy decreases.

The ability of the model to produce energy-dependent lag and/or pulse width is restricted by the requirement for closure between

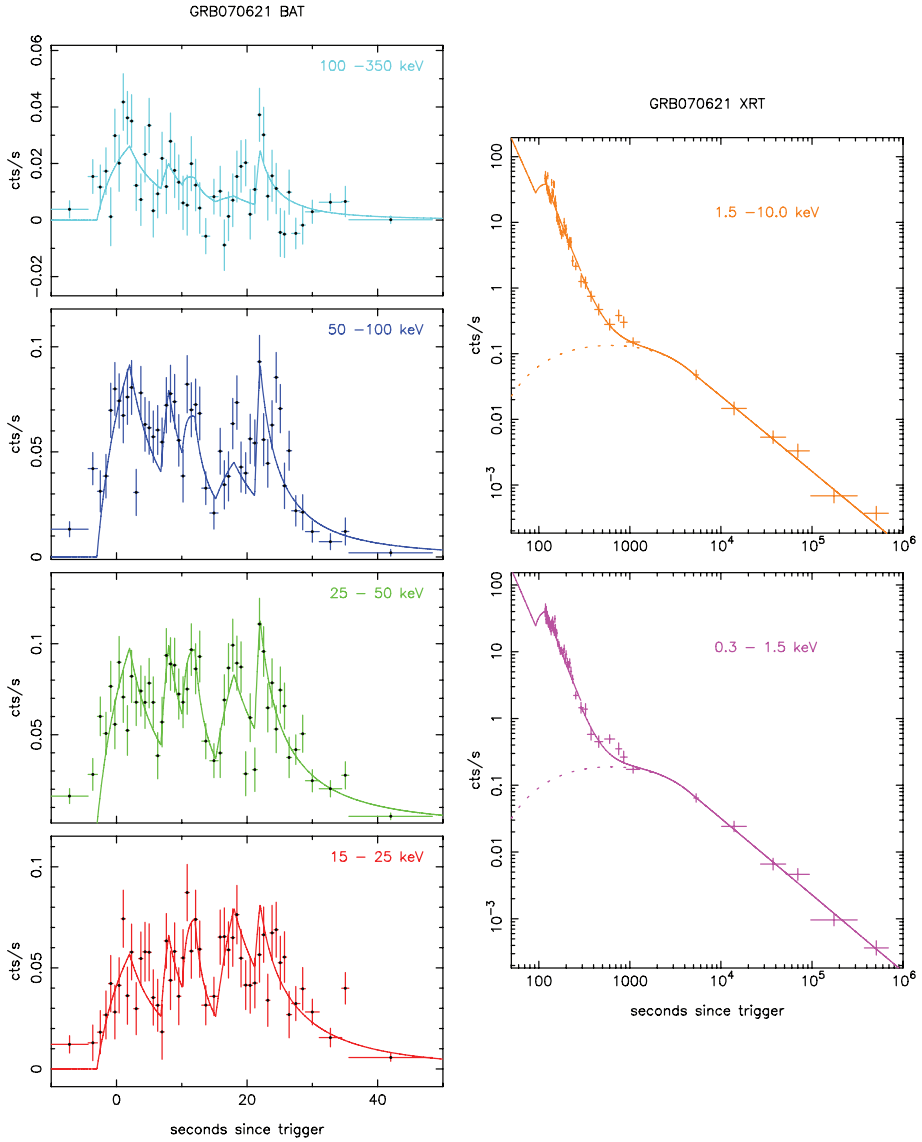

Figure 11. GRB070621.

the temporal decay and spectral indices. If a pulse is bright in the hard energy band, the spectral index tends to be close to zero but this in turn tends to produce a slow initial decay of the hard pulse. Conversely, if the pulse is soft then the spectral index is large and negative and we expect a fast initial decay in the soft band. It may be possible to fit the lag/narrowing seen in pulses like the first pulse of 080805 or the hard peak of the second pulse of 060814 using two pulse components rather than just one. However, such component pulses would overlap to a large degree and the parameters of the pulses should be coupled in the fitting procedure to prevent the result becoming unphysical. This was not attempted in the present work.

Our model is rather simplistic and does not include specific physical details associated with, for example, the internal shocks. When two shells collide, there will be two emission regions, corresponding to the shocked portions of each shell, and they can have the same onset time, $T_{\rm ej} + T_0$, the same R_0 and Γ ($R \geq R_0$) but different emission conditions, $E_{\rm peak}$ or ΔR, and different peak times, $T_{\rm ej} + T_f$. We assume the simplest possible history for each shell, that it has coasted at the same Γ since it was ejected, and retains the same Γ when emitting. In practice multiple collisions are possible and the value of Γ during the emission can be different than before. It can be increased or decreased due to the collision with the second shell that triggers the emission or some deceleration of the front shell due to the sweeping up of the external medium may also occur. The emission may not be caused by internal shocks and may not be synchrotron so the values of indices $a = 1$ and $d = -1$ might be inappropriate. All these factors will clearly modify the pulse profile and spectrum and the way pulses overlap.

There are three parameters which were allowed to float in the fitting for all the pulses; the peak flux F_f, the characteristic time T_f and the spectral index b_1. We have used b_1 in conjunction with E_f to calculate the peak energy $E_{\rm peak}$ which, as introduced in Band et al. (1993), is a measure of the spectral hardness. The distribution of these parameter values are shown in Fig. 15. The top-left panel shows T_f versus the peak time T_{pk}. Somewhat surprisingly, there is no strong correlation between the position of the peak with respect to the trigger time and length of the pulse although there is a consistent trend for the later peaks, $T_{pk} > 50$ s. So within the prompt phase the time-scale of the pulses as measured by T_f is not dictated by the time

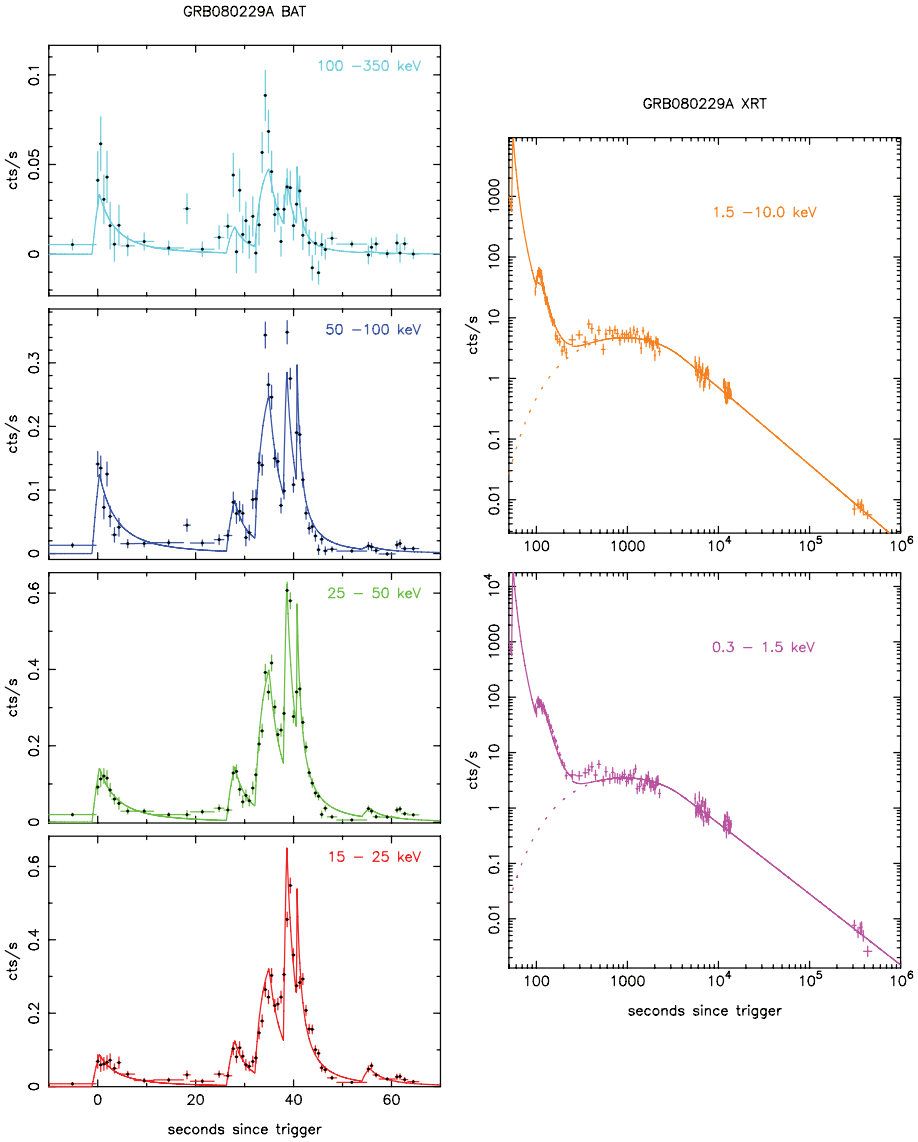

Figure 12. GRB080229A.

since the start of the burst. The sequence of T_f values for 061121 is a good example of this. The top-right panel shows the correlation between T_f and the peak flux F_f. Here is an obvious trend which includes the late, weak flare seen by the XRT in 050724. Similar correlations were discussed by Lee, Bloom & Petrosian (2000) and Quilligan et al. (2002) although they were considering the pulse width rather than T_f. We demonstrate later in this section that T_f is in fact closely correlated with pulse width. The first survey of X-ray flares seen in GRBs, Chincarini et al. (2007), reports a correlation between the flare flux and time of flare since the trigger. Again, this is clearly related to the $F_f - T_f$ correlation although we have shown that T_f is not well correlated with the time since trigger for early pulses. The bottom panels show the peak energy $E_{\rm peak}$, plotted against T_f (left-hand panel) and F_f (right-hand panel). The points for which an error range in E_f was calculated are marked in red. For $T_f > 10$, the peak energy clearly drops with increasing T_f and $E_{\rm peak}$ is also correlated with the peak flux, F_f.

Table 2 also includes an estimate of the peak luminosity of the pulses for those bursts with a measured redshift. Because the peak flux, F_f, is correlated with T_f, as shown in Fig. 15, the luminosity, L_f, is similarly correlated with the characteristic pulse time in the source frame, $T_f/(1+z)$, as shown in Fig. 16. The best-fitting correlation line plotted is $L_f = 1.3 \times 10^{53}\,[T_f/(1+z)]^{-2.0\pm0.2}\,{\rm erg\,s^{-1}}$. The most luminous pulse is the fifth pulse in 061121 with $T_f/(1+z) = 0.7$ s and $L_f = 2.6 \times 10^{53}\,{\rm erg\,s^{-1}}$ while the least luminous prompt pulses (ignoring the late flare in 050724) were soft and only seen in the XRT, for example the second pulse of 050724 with $T_f/(1+z) = 53$ s and $L_f = 3.7 \times 10^{48}\,{\rm erg\,s^{-1}}$. A very similar correlation between X-ray flare luminosity and time of flare since the GRB was presented by Lazzati, Perna & Begelman (2008). They were considering the time since trigger of the peak of the flare, referred to as T_{pk} here, but for late flares seen in the XRT this is very similar to T_f. A correlation between T_f and T_{pk} for the later prompt pulses, $T_{pk} > 100$ s, is evident in the top-left panel of Fig. 15. Assuming that T_{pk} is a good proxy for T_f for the flares analysed by Lazzati et al. (2008), the values derived here extend the relation down to $T_f/(1+z) = 1$ s. From this perspective, the prompt pulses and late X-ray flares may form a continuum consistent with a common origin associated directly with activity in the central engine. We note that the power-law index derived by Lazzati et al. (2008),

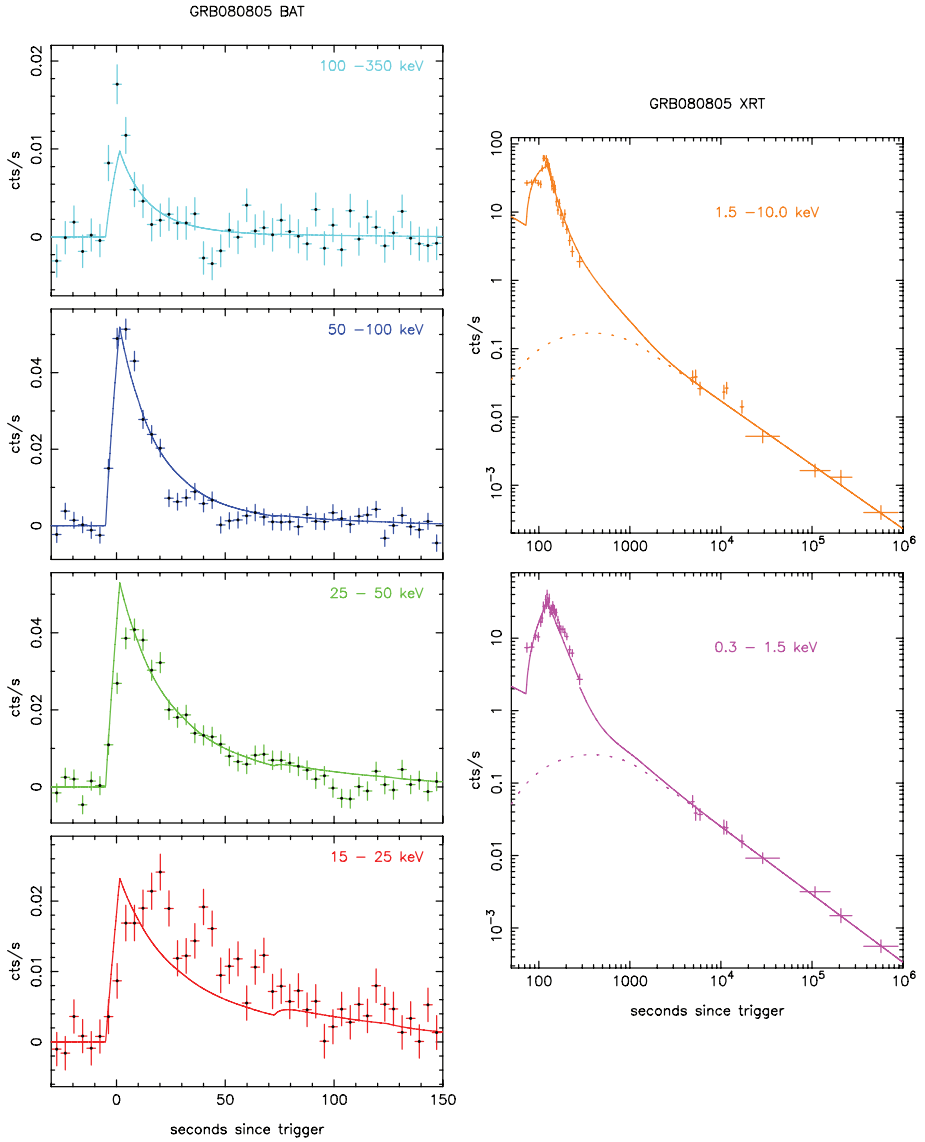

Figure 13. GRB080805.

$\alpha = -1.5 \pm 0.16$, is a little shallower than the value of -2.0 ± 0.19 here although this may be due to the small number of pulses/flares included in the analysis. For early prompt pulses, there is no correlation between T_{pk} and T_f (Fig. 15, top-left panel) so the extended correlation only makes sense if we consider the time since ejection of the pulses not the time since the start of the burst. If this is the case, the arguments that the correlation is associated with accretion, $L \propto \dot{m} \propto t^{-1.2}$, or alternatively with the spin-down of a magnetar, $L \propto t^{-2}$, are not appropriate. A more detailed analysis incorporating a far larger number of prompt pulses and flares is required to see if they really do obey a simple power-law correlation over the entire range $1 < T_f < 10^4$ s or whether the prompt pulses and late flares form two distinct populations indicating that they arise from different mechanisms.

A significant correlation of L_f with the peak energy of the spectrum in the source frame, $E_{\rm peak}(1+z)$, is also shown in Fig. 16. The best-fitting correlation plotted is $L_f = 6.1 \times 10^{46}$ $(E_{\rm peak}(1+z)\,{\rm keV})^{1.83\pm0.16}$ erg s^{-1}. This correlation is similar to the luminosity–peak energy relation reported by Yonetoku et al. (2004), but here we stress that we are considering individual pulses and not the average behaviour of bursts. The correlation is between the luminosity at a particular time (T_f seconds after ejection when the emission suddenly turns off) and the peak energy at exactly the same time indicating a strong physical link between the these quantities. A spectral–luminosity relation within individual *Fermi* GRBs has also been reported by Ghirlanda, Nava & Ghisellini (2009). The correlation they find is consistent with the values reported here and with the peak–energy luminosity correlation for long bursts discussed by Nava et al. (2008). Krimm et al. (2009) provide spectral fits with estimates of $E_{\rm peak}$ for time intervals within individual bursts (see Table 3 and the Discussion) but they concern themselves with the $E_{\rm peak} - E_{\rm iso}$ relation rather than correlation with the peak luminosity.

The rise time of the pulse, $T_{\rm rise}$, was also included in the fitting although in many cases it was fixed because the data were not good enough to determine a useful error range. The left-hand panel of Fig. 17 shows a strong correlation between the rise time and the characteristic time T_f. As expected $T_{\rm rise}$ is always less than T_f in accordance with the definitions illustrated in Fig. 1. This result was not included as a constraint in the fitting but arises from the shape of

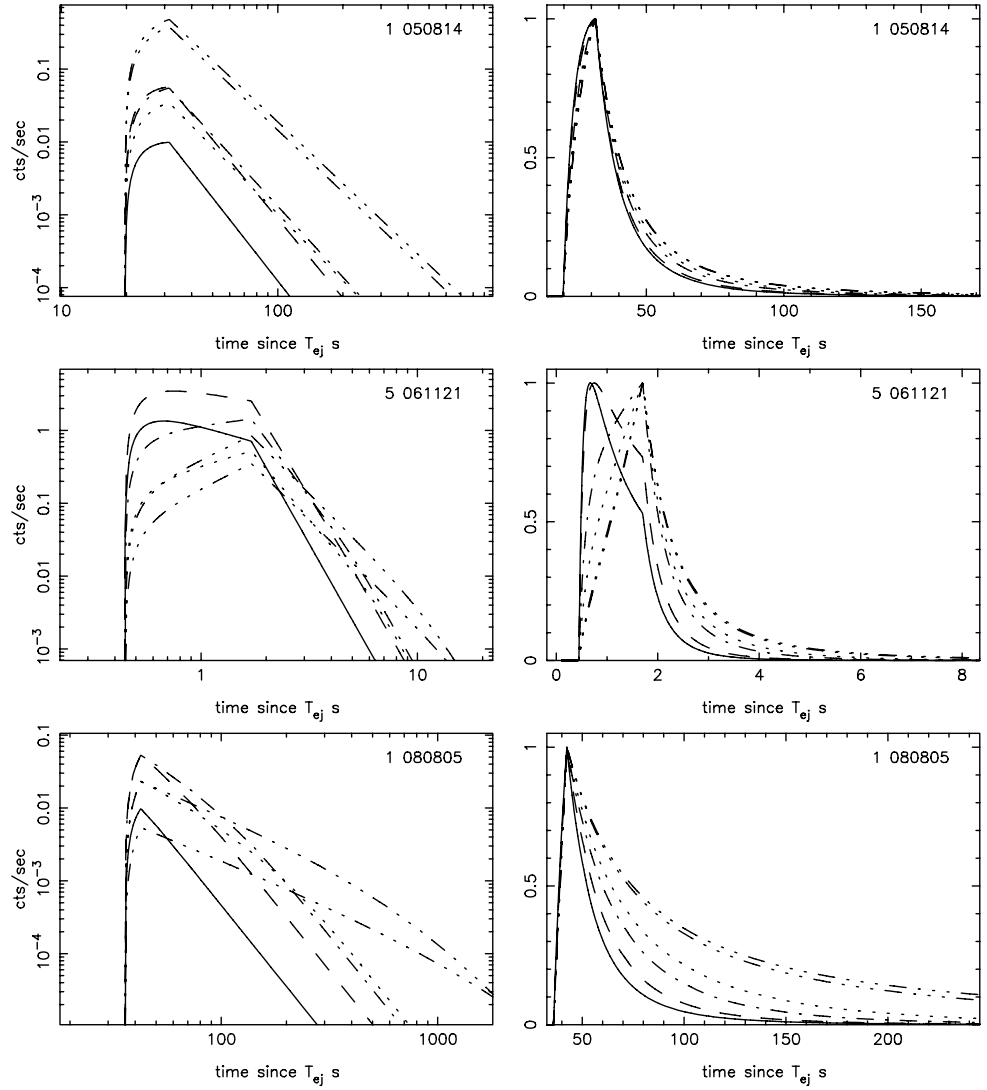

Figure 14. Pulse profiles as a function of energy band. Top panels: pulse 1 of 050814, a typical pulse. Middle panels: pulse 5 of 061121 which exhibits energy dependent lag. Bottom panels: pulse 1 of 080805 which exhibits energy dependent pulse width. Left-hand panels: the count rate versus time since $T_{\rm ej}$ with logarithmic scales. The XRT rates have been divided by a factor of 1000 to put them in the same range as the BAT rates. Right-hand panels: the count rates have been scaled to a fixed value of 1 at T_f seconds after $T_{\rm ej}$ and axes are now linear. In all panels: BAT 100–350 keV (solid), BAT 50–100 keV (dashed), BAT 25–50 keV (dash–dotted), BAT 15–25 keV (dotted), XRT 1.5–10 keV and 0.3–1.5 keV (both dash–dot–dot–dot).

the pulses fitted. Because of this strong correlation, the distribution of $T_{\rm rise}$ with respect to the other parameters are very similar to those of T_f shown in Fig. 15. The right-hand panel of Fig. 17 shows the distribution of the ratio $T_{\rm rise}/T_f$ with respect to T_f. This ratio is closely related to the distance the shell moves during the emission relative to the radius of the shell at the start of the emission (Genet & Granot 2009), $T_{\rm rise}/T_f = \Delta R/(R_0 + \Delta R)$. There is no correlation between this ratio and the other parameters.

The time from the ejection of the shell to its peak is physically the time when the emission from the shell switches off at radius R_f and thus determines the decay time of the peak, which in turn usually dominates the width of the pulse. So, while T_f cannot be measured directly because the ejection of the shell is not observed the width of the pulse largely dictates the value of T_f in the fitting and we expect this time to be correlated with the full width at half-maximum (FWHM) of the pulses which is directly measurable. The FWHM of the pulses is a complicated function of T_f, $T_{\rm rise}$, the spectral parameters b_1, E_c and $b_1 - b_2$ and the observed spectral band so we have estimated it by numerical interpolation for the lowest energy band of the BAT. The left-hand panel of Fig. 18 shows the FWHM plotted against T_f clearly showing the expected correlation. Note that the FWHM is always less or equal to T_f. The right-hand panel shows the FWHM versus the time of peak since the trigger, T_{pk}. In this case, there is no correlation because the pulse width or T_f are not related to the time since the start of the burst. Because of the tight correspondence between pulse width and T_f, any correlations involving T_f presented here also hold if we substitute the observed FWHM for the fitted value of T_f. Similarly, we expect the correlations and analysis involving the FWHM of flares given elsewhere, for example in Chincarini et al. (2007), could be interpreted in terms of T_f.

6 CONCLUSIONS

To summarize, we have successfully fitted the spectrally resolved light curves of 12 GRBs using an analytical expression for pulse

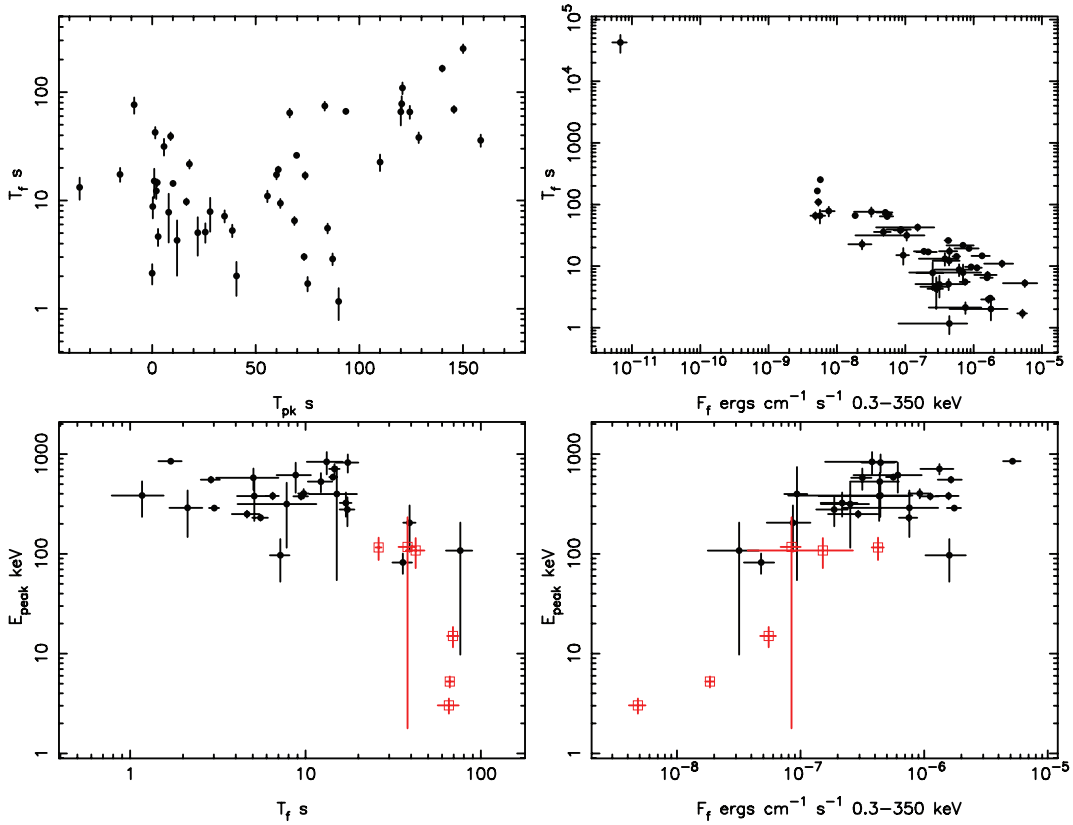

Figure 15. The fitted parameter distributions. Top-left panel: the characteristic pulse time, T_f, versus the position of the peak with respect to trigger time, T_{pk}. The late flare in 050724 has been omitted because T_{pk} can be negative and therefore cannot be plotted on a logarithmic scale. Top-right panel: T_f versus the peak flux F_f. Bottom-left panel: the peak energy $E_{\rm peak}$ versus T_f. Bottom-right panel: the peak energy $E_{\rm peak}$ versus F_f. The fits for which an error range in E_f was calculated are shown as squares (red).

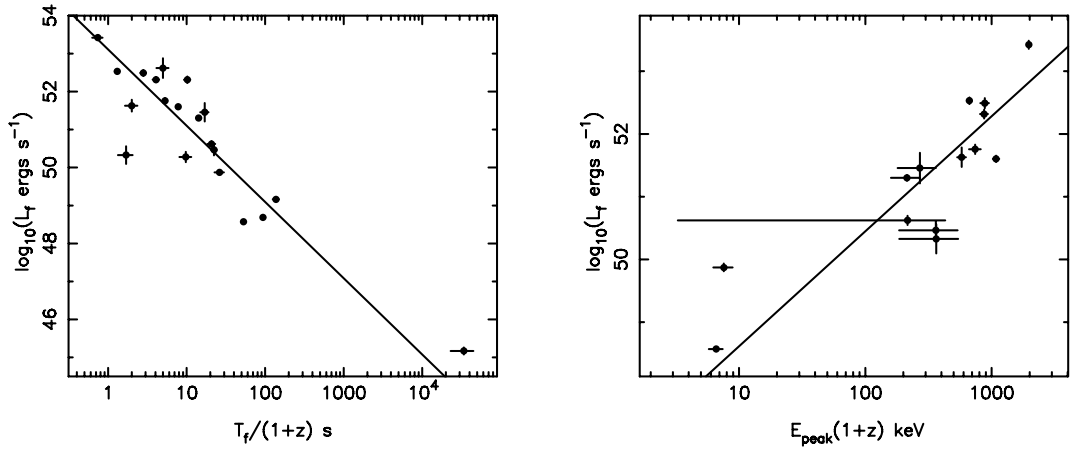

Figure 16. Left-hand panel: the luminosity at the peak of the pulse L_f erg s^{-1} versus the characteristic pulse time in the source frame, $T_f/(1+z)$. Right-hand panel: the luminosity at the peak of the pulse L_f erg s^{-1} versus the peak energy of the spectrum in the source frame, $E_{\rm peak}(1+z)$.

profiles derived from the internal shock model incorporating the spectrum and decay indices expected from synchrotron emission in the fast cooling regime and a decay tail arising from HLE. A total of 49 pulses describe all the major features through the prompt emission into the RDP and, in one case, a late X-ray flare. In all cases, the fit to the RDP is good and there is no doubt that the HLE can account for this phase of the emission from GRBs. In many cases, the energy-dependent pulse profile is as predicted by the model showing elements of spectral lag and spectral pulse broadening and indicating that the spectral evolution incorporated in the model is in agreement with observations. There are aspects of the data which are not in accordance with the simple model. One short, hard pulse in 061121 required index $a = 2.4$, much higher than the value expected for synchrotron emission, $a = 1$. Several pulses have a hard peak which cannot be adequately fitted. There is one pulse, the fourth in 060814, which has a narrow hard peak and broad soft tail which could not be represented by one pulse but had to be split into two components. In the present procedure, the pulses were

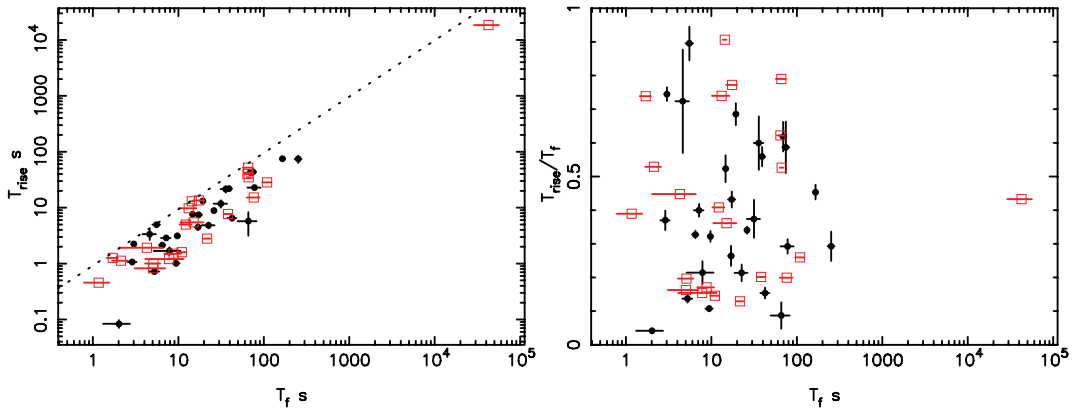

Figure 17. The rise time parameter $T_{\rm rise}$. Left-hand panel: $T_{\rm rise}$ versus T_f. The dotted line indicates equality. Right-hand panel: the ratio $T_{\rm rise}/T_f$ versus T_f. The points with no error bars for $T_{\rm rise}$ (i.e. fixed in the fitting) are plotted as squares (red).

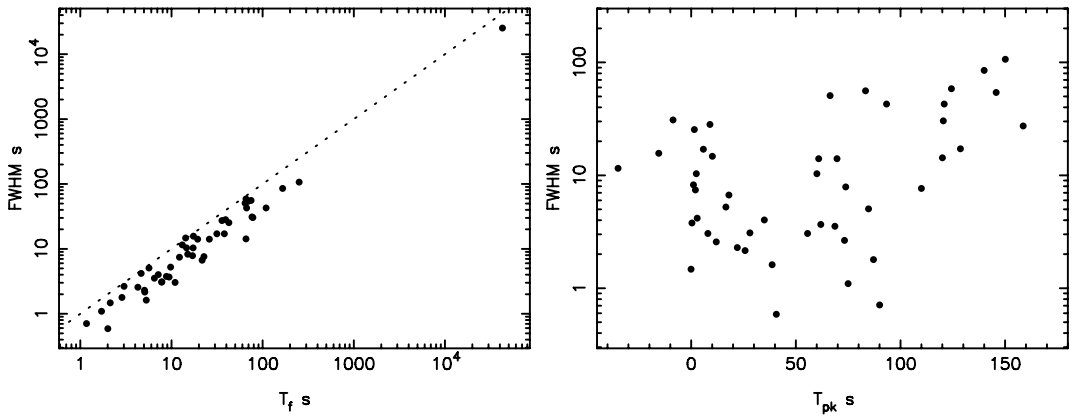

Figure 18. The FWHM of the pulses in the BAT energy band 15–25 keV. Left-hand panel: the FWHM versus the characteristic time T_f. The dotted line indicates equality. Right-hand panel: the FWHM versus the time since trigger of the peak, T_{pk}.

fitted independently with no constraints between the parameters of individual pulses. Future modelling should include such constraints so that the overlap of the pulses remains physically possible. We find that the luminosity of pulses is anticorrelated with the time since ejection for the pulses such that bright pulses arise when the time since ejection is small while the dim pulses correspond to long times since ejection. The individual pulse luminosity is also correlated with the peak energy of the pulse spectrum consistent with the known correlation of peak luminosity for the entire burst with the peak energy of the T_{90} spectrum.

ACKNOWLEDGMENTS

RW and PTO gratefully acknowledge STFC funding for *Swift* at the University of Leicester. JG gratefully acknowledges a Royal Society Wolfson Research Merit Award.

REFERENCES

Arnaud K. A., 1996, in Jacoby G. H., Barnes J., eds, ASP Conf. Ser. Vol. 101, Astronomical Data Analysis Software and Systems V, XSPEC: The First Ten Years. Astron. Soc. Pac., San Francisco, p. 17
Band D. et al., 1993, ApJ, 413, 281
Barthelmy S. D. et al., 2005, Space Sci. Rev., 120, 143
Bloom J. S., Perley D. A., Chen H. W., 2006, GCN Circ., 5826, 1
Burrows D. N. et al., 2005, Space Sci. Rev., 120, 165
Butler N. R., Kocevski D., 2007, ApJ, 663, 407
Chincarini G. et al., 2007, ApJ, 671, 1903
Fynbo J. P. U., Thoene C. C., Malesani D., Hjorth J., Vreeswijk P. M., Jakobsson P., 2007, GCN, 6759, 1
Gehrels N. et al., 2004, ApJ, 611, 1005
Genet F., Granot J., 2009, MNRAS, 399, 1328
Ghirlanda G., Nava L., Ghisellini G., 2009, A&A, submitted (arXiv:0908.2807)
Granot J., 2005, ApJ, 631, 1022
Granot J., Cohen-Tanugi J., do Couto e Silva E., 2008, ApJ, 677, 92
Jakobsson P. et al., 2006, in Holt S. S., Gehrels N., Nousek J. A., eds, AIP Conf. Ser. Vol. 836, Gamma-Ray Bursts in the Swift Era: Sixteenth Maryland Astrophys. Conf. Am. Inst. Phys., New York, p. 552
Jakobsson P., Fynbo J. P. U., Vreeswijk P. M., de Ugarte Postigo A., 2008, GCN, 8077, 1
Krimm H. A. et al., 2009, ApJ, 704, 1405
Kumar P., Panaitescu A., 2000, ApJ, 541, L51
Lazzati D., Perna R., Begelman M. C., 2008, MNRAS, 388, L15
Lee A., Bloom E. D., Petrosian V., 2000, ApJS, 131, 1
Nava L., Ghirlanda G., Ghisellini G., Firmani C., 2008, MNRAS, 391, 639
Norris J. P., Bonnell J. T., Kazanas D., Scargle J. D., Hakkila J., Giblin T. W., 2005, ApJ, 627, 324
Norris J. P., Marani G. F., Bonnell J. T., 2000, ApJ, 534, 248
Nousek J. A. et al., 2006, ApJ, 642, 389
O'Brien P. T. et al., 2006, ApJ, 647, 1213
Page K. L. et al., 2007, ApJ, 663, 1125
Prochaska J. X., Bloom J. S., Chen H.-W., Hansen B., Kalirai J., Rich M., Richer H., 2005, GCN, 3700, 1
Quilligan F., McBreen B., Hanlon L., McBreen S., Hurley K. J., Watson D., 2002, A&A, 385, 377

Reichart D. E., Lamb D. Q., Fenimore E. E., Ramirez-Ruiz E., Cline T. L., Hurley K., 2001, ApJ, 552, 57
Sari R., 1998, ApJ, 494, L49
Thoene C. C., Perley D. A., Bloom J. S., 2007, GCN, 6663, 1
Vaughan S. et al., 2006, ApJ, 639, 323
Willingale R. et al., 2007, ApJ, 662, 1093
Yonetoku D., Murakami T., Nakamura T., Yamazaki R., Inoue A. K., Ioka K., 2004, ApJ, 609, 935
Zhang B.-B., Liang E.-W., Zhang B., 2007, ApJ, 666, 1002

This paper has been typeset from a TEX/LATEX file prepared by the author.